Evolution of multicellular longitudinally dividing oral cavity symbionts (*Neisseriaceae*)

Sammy Nyongesa
INRS-Centre Armand-Frappier Santé Biotechnologie
Philipp Weber
University of Vienna https://orcid.org/0000-0002-1577-2690
Eve Bernet
INRS-Centre Armand-Frappier Santé Biotechnologie
Francisco Pullido
INRS-Centre Armand-Frappier Santé Biotechnologie
Marta Nieckarz
Department of Molecular Biology and Laboratory for Molecular Infection Medicine Sweden (MIMS)
https://orcid.org/0000-0002-3813-4923
Marie Delaby
University of Geneva
Cecilia Nieves
INRS-Centre Armand-Frappier Santé Biotechnologie https://orcid.org/0000-0001-7324-1663
Tobias Viehboeck
University of Vienna https://orcid.org/0000-0002-7128-3461
Nicole Krause
University of Vienna
Alex Rivera-Millot
Institut Pasteur de Lille
Arnaldo Nakamura
INRS - Armand-Frappier Sante Biotechnologie https://orcid.org/0000-0002-0777-7790
Norbert Vischer
University of Amsterdam
Michael VanNieuwenhze
Indiana University Bloomington https://orcid.org/0000-0001-6093-5949
Yves Brun
University of Montreal https://orcid.org/0000-0002-9289-1909
Felipe Cava
The laboratory for Molecular Infection Medicine Sweden (MIMS), Department of Molecular Biology. Umeå University. Umeå.
Silvia Bulgheresi (silvia.bulgheresi@univie.ac.at)

University of Vienna https://orcid.org/0000-0002-1441-7152

Frédéric Veyrier

INRS https://orcid.org/0000-0002-8574-0547

Article

Keywords:

Posted Date: January 20th, 2022

DOI: https://doi.org/10.21203/rs.3.rs-1200288/v1

Version of Record: A version of this preprint was published at Nature Communications on August 22nd, 2022. See the published version at https://doi.org/10.1038/s41467-022-32260-w.

Abstract

In spite of the staggering number of bacteria that live associated with animals, the growth mode of only a few symbionts has been studied so far. Here, we focused on multicellular longitudinally dividing (MuLDi) *Neisseriaceae* occurring in the oral cavity of mammals and belonging to the genera *Alysiella*, *Simonsiella* and *Conchiformibius.* Firstly, by applying comparative genomics coupled with ultrastructural analysis, we inferred that longitudinal division evolved from a rod-shaped ancestor of the *Neisseriaceae* family. Secondly, transmission electron microscopy on cells and sacculi showed that, within each *A. filiformis*, *S. muelleri* or *C. steedae* filament, neighbouring cells are attached by their lateral cell walls. Thirdly, by applying a palette of peptidoglycan metabolic precursors to track their growth, we showed that *A. filiformis* septates in a distal-to-proximal fashion. In *S. muelleri* and *C. steedae*, instead, septation proceeds synchronously from the host-attached poles to midcell. Strikingly, based on confocal-based 3D reconstructions, PG did not appear to be inserted concentrically from the cell periphery to its centre, but as a medial sheet guillotining each cell. Finally, comparative genomics revealed MuLDi-specific differences that set them apart from rod-shaped members of the *Neisseriaceae*. These MuLDi-specific genetic differences comprise the acquisition of the amidase-encoding gene *amiC2*, the loss of *dgt, gloB*, *mraZ* (an activator of the *dcw* cluster), *rapZ*, and amino acids changes in 7 proteins, including the actin homolog MreB and FtsA. Strikingly, introduction of *amiC2* and allelic substitution of *mreB* in the rod-shaped *Neisseria elongata* resulted in cells with longer septa.

In conclusion, we identified genetic events that may have allowed rod-shaped *Neisseriaceae* to evolve multicellularity and longitudinal division. The morphological plasticity of *Neisseriaceae* together with their genetic tractability, make them archetypal models for understanding the evolution of bacterial shape, as well as that of animal-bacterium symbioses.

Introduction

Allometry of animal-microbe associations suggests that 10^{25} prokaryotes thrive on animals and 10^{23} on humans (Kieft and Simmons, 2015; Whitman et al., 1998) and, yet, the morphology and growth mode of animal symbionts are underexplored (Bulgheresi, 2016). Although many may form biofilms (see for example Buskermolen et al., 2016; Kosten et al., 2015), intestinal segmented filamentous bacteria (SFB; Hampton and Rosario, 1965; Jonsson et al., 2020; Schnupf et al., 2015) and three genera of *Neisseriaceae* that occur in the oral cavity (e.g., species belonging to the genera *Alysiella*, *Simonsiella* and *Conchiformibius*; Hedlund and Kuhn, 2006; Hedlund and Tønjum, 2015; Kuhn et al., 1978; Xie and Yokota, 2005), are the only known animal symbionts that may be regarded as multicellular, i.e. they invariably form stable filaments of more than two cells. SFB occur in the small intestine of several animals and play a primal role in pathogen resistance and gut homeostasis (Ericsson et al., 2014; Schnupf et al., 2017). In contrast to SFB, multicellular oral cavity *Neisseriaceae* are relatively understudied. They are closely related to the other » 30 species of *Neisseriaceae* occurring, for the majority, in the buccal cavity of warm-blooded vertebrates, they are cultivable and some are genetically tractable (Nyongesa et al., n.d. submitted publication; Veyrier et al., 2015). Besides multicellular, *Neisseriaceae* may be rod-shaped (e.g.,

Neisseria elongata) or coccoid (e.g., the human pathogen *Neisseria meningitidis* and *Neisseria gonorrhoeae*). *A. filiformis* cells are 2 µm-long and 0.6 µm-wide on average and form upright-standing palisades on the squamous epithelium of the mouth, so that each cell has a proximal pole attached to the host epithelium and a distal, free pole (Figures 1, 2B). Furthermore, within each filament, *A. filiformis* cells appear as paired. Concerning *S. muelleri* and *C. steedae* (previously known as *Simonsiella steedae*; Kuhn et al., 1978), they are thinner, but can be up to 4 and 7 µm-long, respectively. Unlike *A. filiformis,* both poles of *S. muelleri* and *C. steedae* are attached to the mouth (Kuhn et al., 1978; Pangborn et al., 1977). This confers *S. muelleri* and *C. steedae* cells a curved (or crescent-shaped) morphology and we will henceforth refer to their host-attached poles as proximal and to their midcell as their most-distal region (Figure 1 and Figure 2C-D). Although fimbriae were detected on the proximal pole of *A. filiformis* (G. E. Kaiser and Starzyk, 1973) and on the host-proximal side of *S. muelleri* (previously referred to as ventral or concave side; Pangborn et al., 1977), up to this study, *C. steedae* fimbriae localization pattern was unknown.

Besides multicellularity, another peculiarity of *Alysiella*, *Simonsiella* and *Conchiformibius* is that they divide longitudinally (Gary E Kaiser and Starzyk, 1973; Kuhn et al., 1978; Murray et al., 1965 and this manuscript). This is extraordinary, given that, except for nematode (Leisch et al., 2016, 2012), insect (Ramond et al., 2016) and dolphin symbionts (Dudek et al., 2021), rod-shaped bacteria typically elongate and divide by transverse fission, two processes coordinated by the elongasome and divisome, respectively. In model bacteria, each of these machineries is constituted by over a dozen proteins, with the actin homologue MreB and the tubulin homologue FtsZ, respectively, orchestrating cell elongation and division (Szwedziak and Löwe, 2013): deletion of *ftsZ* results in filamentation (Bi and Lutkenhaus, 1991), whereas inactivation of *mreB* turned rods into cocci (Höltje, 1998; Veyrier et al., 2015). Even more striking was the effect of specific amino acid changes: in MreB, they resulted in irregularly sized, bent or branched *Escherichia coli* cells (Shi et al., 2018, 2017) and, when affecting FtsZ, they led to misplaced septa in *E. coli*, *Bacillus subtilis* and *Streptomyces* spp. (Addinall and Lutkenhaus, 1996; Monahan et al., 2009; Sen et al., 2019). Curiously, single amino acid mutations in the FtsZ-binding protein Ssg resulted in longitudinally dividing *Streptomyces* (Xiao et al., 2021). Collectively, these findings led to the hypothesis that longitudinal division might have evolved from differential regulation of subtly different MreB and/or FtsZ variants (den Blaauwen, 2018; Thanbichler, 2018).

Here, we sought to find out whether a similar path led to the evolution of *Alysiella*, *Simonsiella* and *Conchiformibius* - henceforth, collectively referred to as multicellular longitudinally dividing (MuLDi) *Neisseriaceae* - by applying comparative genomics to back-track their molecular evolution. To this aim, we closed the genomes of 21 out of 42 *Neisseriaceae* species to obtain a robust phylogeny and correlated it with both ultrastructural analysis and peptidoglycan (PG) mass spectrometry. This approach, which previously identified genetic events underlying the rod-to-coccus transition in the *Neisseriaceae* (Veyrier et al., 2015), revealed that also MuLDi *Neisseriaceae* evolved from a rod-shaped ancestor. Moreover, incubation of *A. filiformis*, *S. muelleri* and *C. steedae* with a palette of fluorescent D-amino acids (FDAAs) revealed that these MuLDi *Neisseriaceae* employ a unique PG insertion pattern to grow.

Indeed, nascent septa cross the cells medially as to guillotine them - from the proximal to the distal pole in *A. filiformis*, or from both poles to midcell in *S. muelleri* and *C. steedae*.

Finally, recapitulation of MuLDi-specific allelic changes in the rod-shaped *N. elongata* resulted in longer septa, suggesting that the transition from transverse to longitudinal division required, at least, the deletion of *mraZ* – here shown to activate the *Neisseriaceae* division cell wall (*dcw*) cluster – the acquisition *amiC2* and MreB amino acid permutations.

The capacity of oral cavity *Neisseriaceae* to have evolved – more than once – into coccoid or MuLDi cells from a rod-shaped ancestor, together with their amenability to cultivability and genetic manipulation, makes them ideal models to understand the evolution of bacterial cell division, as well as that of animal-bacterium symbioses.

Results

Core genome-based phylogeny of *Neisseriaceae* suggests that MuLDi evolved from a rod-shaped ancestor

The *Neisseriales* order comprise the *Chromobacteriaceae* family and the *Neisseriacea*e family. Recently three new families have been suggested (*Aquaspirillaceae; Chitinibacteraceae* and *Leeiaceae*) (Chen et al., 2021). The *Neisseriaceae* family now includes 12 genera (*Alysiella; Bergeriella; Conchiformibius; Eikenella; Kingella; Morococcus; Neisseria; Simonsiella; Snodgrassella; Stenoxybacter; Uruburuella; Vitreoscilla*). We selected species from each of these *Neisseriacea*e genera and used SMRT (PacBio) and Minion (Nanopore) technologies to obtain 21 additional closed genomes (Table S1). Genomes obtained in this study were combined with *Neisseriaceae* draft genomes (n=365) from NCBI database to calculate the Average Nucleotide Identity (ANI) in order to identify the main species corresponding to genomes with ANI>95% (Table S2). We obtained 69 species for the construction of a core genome-based phylogeny using closed genomes or, if not, the draft genome for each species (Figure 1). Phylogeny results were similar to a recently published study (Chen et al., 2021). Of note, although most genomes available in the NCBI database originated from coccoid *Neisseria* (lineage 1; dark blue in Figure 1), the detailed phylogenetic analysis of this lineage, which likely evolved from an ancestral rod (Veyrier et al., 2015) and which include the well-known pathogens *N. meningitidis* and *N. gonorrhoeae*, will be presented elsewhere (Veyrier lab, in preparation).

Using Scanning-Electron Microscopy (SEM), we imaged all the species that are available in public collections to morphologically classify them as rod, cocci or MuLDi. Of note, we used sublethal concentrations of Penicillin G to test the elongation capacity of species that could not be unambiguously classified as rods or cocci by SEM, as previously described (Veyrier et al., 2015). This allowed us to confirm that all *Neisseriaceae* are rod-shaped (bacilli), except for two closely related species (*N. wadsworthii* and *N. canis*; henceforth referred to as coccoid lineage 2, light blue branches in Figure 1), which did not lengthen upon Penicillin G treatment. Remarkably, we found that coccoid species belonging to lineage 2 harbour genes encoding for the elongasome, but lost *yacF/zapD* (Figure 4), a major genetic

event which also allowed the emergence of coccoid lineage 1 (Veyrier et al., 2015). Moreover, most species from the *Chromobacteriaceae* family (which, as aforementioned, belongs to the *Neisseriales* order) are also described as typical rod-shaped cells (Adeolu and Gupta, 2013), which suggests that the shape of the ancestor of all *Neisseriaceae* was a rod.

Collectively, our phylogenetic analysis indicates that two lineages of cocci (coccoid lineages 1 and 2) evolved independently from a rod-shaped ancestor and that two lineages of MuLDi evolved from a rod-shaped ancestor, *Simonsiella/Alysiella* and *Conchiformibius*, referred to as MuLDi lineage 1 and 2, respectively.

MuLDi *Neisseriaceae* are attached by their lateral cell walls and harbour a characteristic signature in their muropeptide composition

Previous (Gary E Kaiser and Starzyk, 1973; Kuhn et al., 1978; Murray et al., 1965), as well as our microscopic analyses (see electron micrographs of cells shown in Figure 1, Figure 2, Figure S1b-d and Supplementary Movies 1-4) suggested that *A. filiformis*, *S. muelleri* and *C. steedae* filaments result from incomplete cell separation. Moreover, Nile red staining confirmed the presence of membranes between adjoining cells (Figure S1e and f). To understand whether adjoining MuLDi *Neisseriaceae* share additional cellular structures, which prevent them to separate from one another, we performed transmission electron microscopy (TEM) of sacculi extracted from *A. filiformis*, *S. muelleri* and C. *steedae*, as well as from the transversally dividing rod-shaped *N. elongata*, for comparison (Figure 2 and Figure S1a). We observed that, the sacculi of the three MuLDi symbionts, even upon extraction, remained attached, laterally, to one another (Figure 2b-d, bottom panels). We concluded that in the *Neisseriaceae A. filiformis*, *S. muelleri* and C. *steedae* multicellularity results from adjoining cells attached by a cell-wall flanked by two inner membranes.

We previously showed that a modification in the PG composition of the *Neisseriaceae* (increased proportion of pentapeptides) accompanied their rod-to-coccus transition (Veyrier et al., 2015). To find out whether the rod-to-MuLDi transition would also correlate with a change in total muropeptide composition, we applied mass spectrometry to analyse the PG of three MuLDi *A. filiformis*, *S. muelleri* and C. *steedae*, as well as that of 14 rod-shaped *Neisseriaceae* (Figure S2). The abundance of dimers (Di), trimers (Tri) and tetramers (Tetra) relative to the abundance of monomers and the estimated total crosslinked were generally higher in MuLDi (Figure S2 c and d). We concluded that, when compared to rod-shaped *Neisseriaceae*, MuLDi *Neisseriaceae* PG was more crosslinked (Figure S2).

Alysiella filiformis nascent septa guillotine the cells from their distal to their proximal poles

Fimbriae-like structures were detected by TEM on the regions of *A. filiformis* attached to oral epithelial cells (Gary E Kaiser and Starzyk, 1973; Murray et al., 1965; Pangborn et al., 1977). To confirm the

presence of fimbriae at the proximal pole, we immunostained them with an anti-fimbriae antibody and found its signal to be localized at the proximal pole, consistent with the seminal ultrastructural data. Moreover, we noticed that, when observed at the epifluorescence microscope, the proximal, fimbriae-rich side of each filament was invariably the convex one (Figure S3 a-d), which allowed us to establish *A. filiformis* polarity in the absence of fimbriae localization in all the following microscopic analyses.

After confirming *A. filiformis* polarity, we proceed to determine its growth mode by tracking PG synthesis by consecutively applying the three fluorescent D-amino acids (FDAAs) HADA (blue), BADA (green) and TADA (red), which are labelled D-Ala residues incorporated into the peptide side chains of new PG. When imaged by epifluorescence microscopy, *A. filiformis* cells sequentially labelled with HADA 30 min, BADA 15 min and TADA 15 min showed strongest fluorescent signal at their septation planes. The virtual time-lapse obtained by the triple FDAAs labelling revealed that *A. filiformis* starts to septate at the distal pole and that PG synthesis is continued unidirectionally toward the proximal cell pole (Figure 2 f, i, k and S4 a-c; Movie S5), consistent with what observed by thin section TEM (Figure 2b). To view the PG insertion pattern in 3D, we performed confocal microscopy (Figure 3). Surprisingly, the septal signal appeared as a sheet when viewed from the side, and, contrarily to what observed in other transversally (Bisson-Filho et al., 2017; Yang et al., 2017) or longitudinally (Pende et al., 2018) dividing bacteria, we did not observe PG discs or arcs at any septation stage.

In conclusion, we showed that *A. filiformis* septation is asynchronous (i.e., it proceeds from the distal to the proximal pole) and non-centripetal, i.e., the PG appeared not to be inserted concentrically, from the periphery to the centre of the cell, but as a sheet that guillotined each cell from its distal to its proximal pole.

Simonsiella muelleri and *Conchiformibius steedae* septation starts at both poles synchronously and proceeds from the poles to midcell

Based on previous ultrustructural studies, *S. muelleri* fimbriae are situated on the cell side facing the epithelial cells (Murray et al., 1965; Pangborn et al., 1977), here referred to as the proximal side. To test whether this was also the case for *C. steedae* cells, we immunostained them with an anti-fimbriae antibody and confirmed that fimbrial appendages covered the proximal (concave) side of each filament (Figure S3c and d).

To understand how they grow, we then tracked the synthesis of PG by subsequently applying HADA (blue), BADA (green) and TADA (red) to *S. muelleri* and *C. steedae*. When imaged by epifluorescence microscopy, *S. muelleri* and *C. steedae* sequentially labelled with HADA 30 min, BADA 15 min and TADA 15 min and with HADA 1h, BADA 45 min and TADA 45 min, respectively, showed strongest fluorescent signal at the septation plane. However, the virtual time-lapse obtained by the triple FDAAs labelling differed from that obtained for *A. filiformis*. Namely, both *S. muelleri* and *C. steedae*, appeared to start

septation at both poles synchronously and PG insertion continued, bidirectionally, until midcell was reached (Figure 2g, h, j and k and Figure S4d-f).

To view the PG insertion pattern in 3D, we performed confocal microscopy on FDAA- labelled *C. steedae* (Figure 3c-e; Movie S6). At septation onset (Figure 3d), FDAA signal appeared as two juxtaposed triangular sheets, each emerging from one cell pole (green signal in septum 1, Figure 3d; red signal indicates the two leading edges). With septation progression, the two leading edges merged at midcell (red oval signal in Figure 3d, septum 2) and finally appeared as a circular disk at the very last septation stage (red signal in septum 3, Figure 3d and S5b).

Summarizing, we propose that the two curved oral symbionts *S. muelleri* and *C. steedae* start septation at each pole independently, but synchronously, and septation ends when the two pole-originated PG sheets meet and merge at midcell.

Multiple genetic events associated with the cell shape transition from rod-shaped to MuLDi *Neisseriaceae*

By applying exhaustive comparative genomics, we previously discovered that mutations at specific genetic loci mediated the rod-to-coccus transition of the ancestor of pathogenic *Neisseria* (Veyrier et al., 2015). We therefore hypothesised that mutations at specific genetic loci, had mediated their evolution from an ancestral, transversally dividing rod-shaped *Neisseriaceae* (Figure 1). Our approach was to detected shared events by the two MuLDi *Neisseriaceae* lineages (the *Simonsiella/Alysiella* lineage 1 and the *Conchiformibius* lineage 2), To identify these genetic loci, we applied previously described pipelines (Guerra Maldonado et al., 2020; Veyrier et al., 2009, 2015) to determine the presence/absence of proteins in 37 species of *Neisseriaceae*, 32 rod-shaped and 5 MuLDi (all displayed in Figure 1). Of note, we excluded both lineages of coccoid *Neisseriaceae* from our analysis, as they underwent a different evolutionary path (Veyrier et al., 2015).

Firstly, we identified 7 genes that were present in MuLDi, but absent in rod-shaped *Neisseriaceae* (Figure 4). These genes comprised a gene encoding for an AmiC-like amidase, henceforth referred to as AmiC2. Interestingly, the *amiC2* gene is always associated with *cdsA*, a gene encoding for the phosphatidate cytidylyltransferase CdsA in all MuLDi species (Figure S6). As *amiC2* and *cdsA* are either flanked by a transposase (in the MuLDi lineage 1) or by a restriction/modification system (in the MuLDi lineage 2), we hypothesize that *amiC2* was acquired by horizontal gene transfer, possibly from a *Fusobacterium*-related bacterium (see AmiC and AmiC-like phylogeny in Figure S7). Intriguingly, Fusobacteria, as the *Neisseriaceae*, are common members of the oral, gastrointestinal and genital flora (Brennan and Garrett, 2018). As for the remaining 6 MuLDi-specific genes, four are predicted to encode for hypothetical proteins and two for the hemolysin transporter ShlB.

Secondly, we found that only 4 genes were absent in MuLDi *Neisseriaceae* when compared to rod-shaped ones (Figure 4). Surprisingly, most of the genes lost during the rod-to-MuLDi transition are implicated in

PG synthesis and cell division (Figure 4a). These genes include: *mraZ* and *rapZ*. *mraZ* is the first gene of the *dcw* cluster (Figure S6) in most bacteria, where it encodes for a poorly characterized, but highly conserved transcriptional regulator MraZ (Eraso et al., 2014; Fisunov et al., 2016; Mengin-Lecreulx et al., 1998). On the other hand, *rapZ* encodes the small RNA adaptor protein RapZ, implicated in cell envelope precursor sensing and signalling (Khan et al., 2020).

Thirdly and lastly, we used our software called CapriB (Guerra Maldonado et al., 2020) to search for amino-acid changes in the 438 proteins strictly conserved among the 39 *Neisseriaceae* species (core proteome) (Figure 4b). Strikingly, we detected amino acid permutations in only 7 out of the 438 proteins (1.6%). Namely, three permutations and two permutations were found in FtsA and MreB, respectively, two proteins which are both involved in bacterial morphogenesis (Busiek and Margolin, 2015). Moreover, we found two permutations in the efflux pump membrane transporter MtrD and one permutation per protein in the DNA-directed RNA polymerase subunit RpoZ, single stranded DNA-binding protein Ssb, two-component regulator MisR and the long-chain-fatty-acid-CoA ligase FadD.

Altogether, comparative genomics of rod-shaped versus MuLDi *Neisseriaceae* identified 18 genetic loci at which mutations might have mediated rod-to-MuLDi transition. Notably, these genetic loci include *mreB*, encoding for the actin homologue, and *amiC2*, encoding for a cell wall amidase.

Downregulation of *dcw* cluster genes in MuLDi *Neisseriaceae*

As several genes encoding for regulators were mutated in MuLDi, we employed RNAseq to determine differential gene expression patterns between MuLDi (n=5) and rod-shaped (n=5) *Neisseriaceae* cultured in the same condition (GCB agar Media, 6h, 37°C 5% CO_2). To compare gene expression between species, we standardized the annotation of the five rod-shaped and the 5 MuLDi *Neisseriaceae* genomes by inferring gene orthology using BlastP. Using NetworkX python programming package (Hagberg et al., 2008), we reannotated clusters of homologous genes in each genome (for example, *ftsZ* gene will be called NEISS_1241 in all the genomes). By doing so, we were able to count the reads associated with each gene in each species and perform DESeq2 statistical analyses using the core transcriptome. Strikingly, our analysis (Figure 4c) showed that the majority of the significantly differentially regulated genes are involved in cell envelope synthesis (as demonstrated by their clustering in the String analysis shown in Figure 4d). Namely, we observed that 12 genes were upregulated in MuLDi species, most notably *minE, ftsX and ftsY* involved in cell division. More importantly, the 19 down-regulated genes in MuLDi species include *ftsA*, *murE* and *ftsI*, which are part of the *dcw* cluster.

To conclude, comparative RNA-seq suggests that the loss of *mraZ* in MuLDi *Neisseriaceae* impacted the expression of *dcw* cluster including *ftsI*.

Downregulation of *dcw* cluster genes in *N. elongata mraZ* deletion mutants

To test whether deletion of *mraZ* in the rod-shaped *Neisseriaceae N. elongata* could cause downregulation of *dcw* cluster genes (similarly to what observed in MuLDi *Neisseriaceae*, that naturally lost *mraZ*), we compared the transcriptomes of wild-type *N. elongate* and a *mraZ* deletion mutant thereof. This revealed that five genes located downstream of *mraZ* (*mraW, ftsL, ftsI, murE* and *murF*) were downregulated (Figure 5a and b). These results were validated by quantitative real-time PCR (Figure 5c). Moreover, overexpressing *mraZ* (by inserting it, ectopically, after the *nrq* locus in the *N. elongata* Δ*mraZ* mutant) restored wild-type expression. Although the *N. elongata* Δ*mraZ* mutant did not display strong morphological defects (Figure 5d), Δ*mraZ pilEp-mraZ N. elongata*, which overexpresses MraZ, tended to be smaller (Figure 5 d and e).

Collectively, we showed that *mraZ* is an activator of transcription of the first five genes of the *N. elongata dcw* cluster, similar to what was proposed for *Mycoplasma* spp. (Eraso et al., 2014).

Recapitulation of MuLDi-specific genetic changes in the rod-shaped *Neisseriaceae Neisseria elongate* resulted in longer septa

After deleting *mraZ*, we tested whether changes at other MuLDi-specific loci could turn the rod-shaped *Neisseriaceae N. elongata* in a MuLDi bacterium. However, as for the *mraZ* deletion, deletion of *dgt, gloB*, or *rapZ* either singularly or in combination did not change *N. elongata* morphology (data not shown). All the same, introduction of *amiC2* (along with its neighbouring gene *cdsA*) in *N. elongata* did not result in significant shape or growth anomalies (Figure 6a), unless it was accompanied by the allelic exchange of *N. elongata mreB* with *S. muelleri mreB,* which resulted in longer cells (Figure 6a and Figure S8).

In a final attempt to turn the rod-shaped *N. elongata* into a MuLDi *Neisseriaceae*, we used an unmarked deletion-based technique developed by us (Nyongesa et al., n.d. submitted) to, concomitantly, delete *dgt*, *gloB*, *mraZ* and *rapZ*, substitute *N. elongata mreB* with *S. muelleri mreB* and introduce *amiC2*/*cds*A. As shown in Figure 6 and Figure S8, *N. elongata* D*dgt*, D*gloB*, D*mraZ,* D*rapZ* with $mreB_{sm}$ cells were longer and branched. More importantly, the substitution of $mreB_{ne}$ with $mreB_{sm}$ together with the introduction of *amiC2/cdsA* resulted in cells which had a longer septum and a shorter axis perpendicular to the septum (Figure 6). Namely, the ratio between the two cell axes changed from 0.61 ± 0.25 (n=186), for the wildtype, to 0.95 ± 0.29 (n=174) for the mutant *N. elongata*.

All in all, even if our attempt to genetically manipulate the rod-shaped *N. elongata* into a MuLDi did not result into a complete transverse-to-longitudinal division switch (ratio between the two cell axes >1), the observed increase in septum length suggests that the genetic events identified by comparative genomics have participated in the rod-to-MuLDi transition in the *Neisseriaceae*.

Discussion

There is a huge discrepancy between the number of known prokaryotic species and how many of them have been characterized morphologically. This makes it hard to predict how the shape and the growth mode of bacteria evolved. In an attempt to fill this knowledge gap, we focused on MuLDi *Neisseriaceae* occurring in the oral cavity of warm-blooded vertebrates, including humans. Whole genome-based phylogenetic analysis, coupled with ultrastructural analysis, indicated that MuLDi *Neisseriaceae* evolved from a rod-shaped, *Neisseriaceae*. Although these rod-shaped septate transversally, our incubations with a set of fluorescently labelled PG precursors showed that MuLDi *Neisseriaceae* septate longitudinally - in *A. filiformis* in a distal-to-proximal fashion, in *S. muelleri* and *C. steedae* synchronously, from both poles to midcell (notably, the other two known species of the *Alysiella* and *Conchiformibius* genera, *A. crassa* and *C. kuhniea*, also septate longitudinally, the former unidirectionally and the latter bidirectionally; Figure S4g). Irrespective of the uni- or bi-directionality of cell wall construction (that remains to be mechanistically deciphered by genomic comparison between *Alysiella* and *Conchiformibius* and *Simonsiella*), we further observed that in these bacteria, new PG was not inserted concentrically, but as a medial sheet guillotining each cell. Finally, full-scale comparative genomics revealed MuLDi-specific differences that set them apart from rod-shaped members of the *Neisseriaceae* (e.g., *amiC2* acquisition, *mraZ* loss and amino acid changes in the cytoskeletal proteins MreB and FtsA). Supporting the role of specific genetic changes in the rod-to-MuLDi transition, introduction of *amiC2* and allelic substitution of *mreB* in the rod-shaped *Neisseriaceae N. elongata* resulted in cells with longer septa.

Taken together, we presented two novel modes of septal growth and we identified genetic events that contributed to the evolution of bacterial multicellularity, longitudinal division and, possibly, host-polarization in a group of mammalian symbionts.

Multiple phylogenetic studies have suggested that the wide palette of bacterial morphotypes we observe today evolved from rod-shaped bacteria, which makes us consider their shape as the ancestral one (Siefert and Fox, 1998; Young, 2006). Our genome-based phylogenetic reconstruction revealed that, even in the *Neisseriaceae*, MuLDi evolved from an ancestral rod-shaped bacterium. It remains uncertain whether these two MuLDi lineages have convergently evolved twice, or whether species belonging to the genus *Kingella* also evolved into MuLDi, but subsequently reverted to the rod-shaped morphology. We speculate that the MuLDi phenotype may have favoured colonisation of- or nutrient uptake from the buccal cavity which is characterized by rapidly shedding epithelial cells and salivary flow (Mark Welch et al., 2020). Indeed, multicellularity makes cooperation among cells possible in the form, for example, of division of labour and may, therefore, help bacteria to survive nutrient stress (see for example Claessen et al., 2014). Although, previous morphological studies suggested that the terminal cells of *S. muelleri* (Hedlund and Tønjum, 2015; Pangborn et al., 1977) and *C. steedae* (Kuhn et al., 1978) might phenotypically differ from the central ones and although we observed a thinner cell every approximately 14 cells in *C. steedae* (Figure S1, S5 and Movie S7), future studies are needed to clarify whether different cell types exist within each filament.

Multicellularity may arise via three distinct processes: aggregation of individual cells resembling the initial stages of biofilm formation (Monds and O'Toole, 2009), the formation of syncytial filaments via crosswalls segmenting the mother cell, but not separating it into daughter cells (streptomycetes; Zhang et al., 2016) and incomplete cell fission after cell division to produce chains of cells (referred to as clustered growth, e.g., filamentous cyanobacteria; Flores et al., 2019). TEM analysis of MuLDi sacculi revealed that these *Neisseriaceae* share one cell wall which makes them resemble to cyanobacteria. If MuLDi cells belonging to the same filament appear to be synchronized (Figure 2 and Figure S4), future studies are needed to find out whether their cytoplasms are connected by septal junctions and/or hemidesmosomes (Flores et al., 2019).

Although longitudinal septation is clearly not a prerequisite of bacterial multicellularity (here defined as clusters of at least 3 cells), these two phenotypic traits appeared to have evolved jointly in the *Neisseriaceae*. Longitudinal septation has also been shown in the nematode symbionts *Candidatus* T. oneisti and T. hypermnestrae (Leisch et al., 2016, 2012), as well as in the fruit fly endosymbiont *Spiroplasma poulsonii* (Ramond et al., 2016). In these three unicellular symbionts, the tubulin homolog FtsZ localized at the septal plane and was therefore thought to mediate septal PG insertion. As for the actin homolog MreB, it was shown to form a medial ring-like structure in *Ca.* Thiosymbion throughout the cell cycle and to be required for septal FtsZ localization and PG insertion (Pende et al., 2018). Indeed, its pharmacological inactivation impaired both *Ca.* Thiosymbion growth and division (Pende et al., 2018). Although the localization pattern of MreB in MuLDi *Neisseriaceae* is currently unknown, its (1) presence in their genomes, (2) its transcriptional expression, (3) the identification of two MuLDi-specific amino acid permutations (H185Q and T247A), and (4) the fact that introducing a MuLDi MreB in the rod-shaped *N. elongata* (with or without the concomitant insertion of the *amiC2* gene) led to shape aberrations suggest that MreB is involved in PG insertion in MuLDi *Neisseriaceae*. Intriguingly, amino acid 185, located after the GVVYS motif, is substituted in MuLDi MreBs when compared to rod-shaped Neisseriaceae (H185Q), but also in longitudinally dividing *Ca.* Thiosymbion when compared to *E. coli* (S185N) (den Blaauwen, 2018). It should also be noted that the allelic substitution of MreB affected differently the morphology of *N. elongata* depending on the genetic background (i.e., presence or absence of other MuLDi-specific genes). This, in addition to the pleiotropic effect of MreB reported in other studies (Shi et al., 2018), can make this protein accountable for accommodating multiple cell shape adaptations (e.g., rod-to-coccus, rod-to-MuLDi). If we still do not know whether MreB and/or FtsZ place the insertion of the PG synthesis machinery at the septum, based on our confocal-based 3D reconstructions, new septal PG is not inserted in successive, concentric rings or ellipses, as shown for model rods (Bisson-Filho et al., 2017; Yang et al., 2017)(Du and Lutkenhaus, 2019) and nematode symbionts (Pende et al., 2018), respectively.

In addition to MreB amino acid changes, MuLDi-specific loss of *mraZ* led to the misregulation of the *dcw* cluster. *mraZ* has been described as a highly conserved transcriptional regulator of the *dcw* cluster, of which *mraZ* is the first gene (Eraso et al., 2014; Fisunov et al., 2016). The *dcw* cluster is a group of genes involved in the synthesis of PG precursors and cell division (Ayala et al., 1994) conserved in most bacterial genomes (Nikolaichik and Donachie, 2000; Tamames et al., 2001; Vicente et al., 1998). Throughout the *Neisseriaceae*, the *dcw* cluster consists of 14-16 tightly packed genes in the same

orientation and mostly in the same order, with *midA* located before the cluster in reverse orientation (Figure S6). The fact that, in the *Neisseriaceae*, the gene content and orientation of the *dcw* cluster mostly mirrored the phylogenetic placement of each species, suggests that the *dcw* cluster evolved vertically. Moreover, having a fragmented *dcw* cluster (as in the case of MuLDi *Neisseriaceae* and some *Kingella* species) does not seem to impact cell morphology, given that both rod-shaped and coccoid species may bear or not bear split *dcw* clusters. Of note, in spite of fragmentation, bacteria can retain some gene sub-clusters (e.g., "*mraW-ftsL, ftsI, murE* and *murF*", "*ftsW, murG*" and "*murC, ddl, ftsQ, ftsA, ftsZ*"), probably because the genes grouped in a given sub-cluster need to be co-transcribed (Mingorance et al., 2004). If several studies agree on the regulatory role of MraZ, its effect seems to vary depending on the organism. In *Neisseriaceae* (this study) and in *Mycoplasma* spp. (Fisunov et al., 2016; Martínez-Torró et al., 2021) it is described as an activator of the *dcw* gene cluster whereas in *E. coli,* MraZ is described as a transcriptional repressor that controls its own expression and that of other *dcw* cluster genes (Eraso et al., 2014). Importantly, deletion or overexpression of MraZ led to cell filamentation in bacteria where MraZ, respectively, activates (e.g., *Mycoplasma* spp.) or represses (e.g., *E. coli*) the *dcw* cluster. If downregulation of the *dcw* cluster did not result in *N. elongata* filamentation, its upregulation, in MraZ-overexpressing *N. elongata*, led to shorter cells. Altogether, our data suggest that, in the *Neisseriaceae*, MraZ is controlling cell elongation via the regulation of the *dcw* cluster and we speculate that it may have altered the balance between the divisome and the elongasome machineries (i.e., in *mraZ*-less MuLDi, the elongasome might contribute to PG synthesis in the septum).

Finally, comparative genomics highlighted the importance of the acquisition of the *cdsA/amiC2* locus. Although its sole deletion does not result in morphological changes of *N. elongata*, when combined with the allelic substitution of $mreB_{sm}$, we observed cells with longer septa. This suggests that the AmiC2 amidase may regulate MuLDi septation. Intriguingly, HPLC analyses of PG extracted from 17 rod-shaped bacteria and from three MuLDi *Neisseriaceae* (*A. filiformis*, *S. muelleri* and *C. steedae*) showed that MuLDi PG is richer in M44 (Figure S2), suggesting higher amidase activity in these *Neisseriaceae*. Concerning the *amiC2*-associated genetic locus *cdsA*, it encodes for a CDP-diacylglycerol synthase putatively implicated in phospholipid biosynthesis. Given that the presence of anionic phospholipids (cardiolipin and phosphatidylglycerol) has been shown to repel MreB (Kawazura et al., 2017), we can hypothesise that CdsA affects the composition of the membrane and, therefore, the localisation of MreB.

Despite all our efforts, we could not turn the rod-shaped *N. elongata* into a complete MuLDi *Neisseriaceae* even upon, concomitantly, replacing MreB, inserting *amiC2/cdsA* and deleting *dgt*, *gloB*, *mraZ* and *rapZ*. This could be due to the fact that we could not recreate all genetic events (such as replacing $ftsA_{ne}$ with $ftsA_{sm}$ due to its proximity to *ftsZ*) or due to the existence of other undetected events (such as species-specific events that resulted in a convergent phenotype).

How could rod-shaped, transversally dividing bacteria evolve into longitudinally dividing ones? Permanent cell shape transitions may have resulted from modifications (e.g., gene deletions, insertions and nucleotide polymorphisms) of genetic loci involved in morphogenesis (e.g., *mreB*, *amiC2*) and, additionally, in those involved in their transcriptional regulation (e.g., *mraZ*). Two evolutionary

scenarios were proposed (den Blaauwen, 2018; Pende et al., 2018; Thanbichler, 2018): (1) an ancestral rod was compressed by its poles so that it got shorter and fatter, or (2) an ancestral rod rotated its septation axis by 90 degrees. Our results suggest that, in the course of evolution, the cell width of an ancestral rod increased (and its length decreased), perhaps following a misbalance between elongation and division. However, genetic tools are needed to gain insights on MuLDi *Neisseriaceae* evolution by, for example, visualizing the localization pattern of FtsZ and MreB or by attempting reversion into unicellular, possibly, transversally dividing bacteria such as *N. elongata*.

To date, most protein function studies have been conducted in either pathogenic or bacterial species that are easy to culture and manipulate in the laboratory such as *E. coli* and *B. subtilis.* In addition to these models, efforts to study other morphologies including commensal species are necessary to understand bacterial cell evolution, but also to increase the pool of protein targets (e.g., antibiotic targets) for industrial and biopharmaceutical applications. Throughout their evolution, *Neisseriaceae* succeeded in repeatedly, and seemingly effortlessly, evolve different cell shapes (e.g., coccoid, MuLDi). Moreover, they are the only known multicellular longitudinally dividing bacteria that may thrive in humans, but which are also cultivable and, likely, genetically tractable. We hence propose the use of *Neisseriaceae* as models to study how longitudinal division and multicellularity evolved as well as the molecular and cell biological mechanisms underlying the establishment of bacterium-animal symbioses.

Materials And Methods

Bacterial strains and culture conditions

The bacterial strains *Neisseria elongata* subsp. *elongata* (DSM 17712), *Alysiella filiformis* (DSM 16848), *Simonsiella muelleri* (DSM 2579), and *Conchiformibius steedae* (DSM 2580) were obtained from the German Collection of Microorganisms and Cell Cultures GmbH (DSMZ). *Neisseria elongata* subsp*. glycolytica* (ATCC 29315) and *Simonsiella muelleri* (ATCC 29453) were obtained from the American Type Culture Collection (ATCC). *N.* sp. DentCa1247 was a gift from Dr. Nathan Weyand (U. of Ohio). For FDAA incubations, western blots, immunostaining and membrane staining, we used BSTSY (*N. elongata, C. steedae*), PY (*A. filiformis*), or meat extract (*S. muelleri*) agar plates that were incubated overnight at 37°C. For all other experiments, bacteria were streaked from -70°C freezer stocks onto Gonococcal culture media supplemented with Kelloggs supplement (GCB) and grown overnight at 37°C in 5% CO_2 incubator. Single colonies were subcultured into the respective liquid media with agitation at 120 rpm and grown to exponential phase (OD_{600} 0.1-0.6). For cloning experiments *E. coli* DH5α cells were cultured onto Luria-Bertani Media at 37^{o}C. When required, antibiotics were used as follows: kanamycin (50 µg/ml for *E. coli*; 100 µg/ml for *N. elongata*), erythromycin (300 µg/ml for *E. coli*; 3 µg/ml for *N. elongata*), chloramphenicol (25 µg/ml for *E. coli*; 5 µg/ml for *N. elongata*), and streptomycin (100 µg/ml for *N. elongata*). Transformation of *N. elongata* was done using linearized plasmid or PCR product by dropping approximately 500 ng of DNA on fresh cultures on GCB media supplemented with 10 mM $MgCl_2$ and incubated for 6-12 hours before subculturing on GCB media containing the appropriate antibiotics and Xgal if needed as described previously (Veyrier et al., 2015).

Time-lapse imaging of *N. elongata*

Strains were streaked from -70°C freezer stocks onto BSTSY agar plates and grown overnight at 37°C with 5% CO2. Single colonies were transferred to liquid culture and grown to exponential phase (OD_{600} 0.2). Cells were spotted onto pads made of 0.8% SeaKem LE Agarose (Lonza, Cat. No. 50000) in BSTSY and topped with a glass coverslip. Cells were transferred to an Okolab stage top chamber to control temperature (37°C) and gas (CO_2 5% and O_2 18%). Images were recorded with inverted Nikon Ti-2 microscopes using a Plan Apo 100X 1.40 NA oil Ph3 DM objective using Hamamatsu Orca FLASH 4 camera. Images were processed with NIS Elements software (Nikon). In all experiments, multiple x/y positions were imaged. Representative images were processed using the Fiji Software package.

Time-lapse imaging of *A. filiformis*, *S. muelleri* and *C. steedae*

Strains were streaked from -70°C freezer stocks onto PY (*A. filiformis*), meat extract (*S. muelleri*) or BSTSY (*C. steedae*) agar plates grown overnight at 37°C with 5% CO2. Single colonies were transferred to liquid culture and grown to exponential phase (OD_{600} 0.2-0.5) at 37°C shaking at 180 rpm agitation. For all strains, 250 µL of diluted exponential phase cultures (OD 0.025) were loaded into the cell loading well of a prepared (shipping solution removed and washed three times with sterile appropriate media) B04A-03 microfluidic plate (Merck-Millipore). Time-lapse imaging was performed using CellASIC® ONIX Microfuidic System. The ONIX manifold was sealed to the B04A-03 plate. CellASIC® ONIX2 System was used as the microfluidics control software. First, a flow program was set up to prime flow channel and culture chamber by flowing medium from inlet wells 1 to 5 at 34.5 kPa for 2 min. Second, cells were loaded onto the plate at 13.8 kPa for 15 s. Priming run was performed for 5 min with pressure set to 34.5 kPa. The medium flow was set at 12 kPa throughout the experiment for 12h with sterile appropriate media. Images were recorded with an inverted Nikon Ti-E microscope using a Plan Apo 60XA oil Ph3 DM objective using Hamamatsu Orca FLASH 4 camera. Images were processed with NIS Elements software (Nikon). In all experiments, multiple x/y positions were imaged. Representative images were processed using the Fiji Software package.

Electron microscopy

For transmission electron microscopy, half a loopful of 6-8 h old bacterial cultures were fixed by direct resuspension in 500 µl of 2.5% glutaraldehyde in 0.1 M cacodylate buffer and incubated for at least 1h at 4°C. Cells were then pelleted through centrifugation at 5000 rpm for 3 min and washed 3 times in 500 µl 0.2 M cacodylate wash buffer solution (PH 7.2). 30-50 µl of wash solution containing bacterial cells was pipetted onto Formvar Carbon 200 mesh copper grids (Sigma-Aldrich) and negative staining done using

1% phosphotungstic acid (PTA) for 2 sec before imaging at the INRS-CAFSB platform using a Hitachi H-7100 electron microscope.

For scanning electron microscopy, fresh bacterial cells were cultured for 6h in liquid media containing poly-L-Lysine (Sigma) coated glass slides. Cells were fixed using 2.5% glutaraldehyde in 0.1 M cacodylate buffer for 1h at 4°C then rinsed 3 times in 0.2 M cacodylate wash buffer solution (PH 7.2). Post fixation was subsequently done using 1% osmium tetroxide (in 0.2 M cacodylate) before gradual dehydration through increasing ethanol concentrations (25%, 50%,75%, 95% and 100%). Carbon dioxide critical point drying (CPD) and gold sputtering were done on Leica EM CPD300 and Leica EM ACE600 instruments respectively. The imaging was done at the electron Imaging Facility (Faculty of dental medicine, Université de Montréal, Québec, Canada) using a Hitachi Regulas 8220 electron microscope.

Peptidoglycan extraction and analysis

Peptidoglycan extraction was performed as previously described (Veyrier et al., 2015). Bacterial cultures were harvested from solid agar plates using inoculation loops and emulsified in 10 ml of distilled water, the suspension mix was added drop by drop into 10 ml of 8% boiling sodium dodecyl sulfate (SDS) and boiled for and extra hour. After overnight storage at room temperature, the cells were washed six times using distilled water (pH 6.0) through ultracentrifugation at 39000 x g for 30 min. The final pellet was lyophilized and resuspended in distilled water (concentration 6mg/ml or more) and stored at –20°C until further use. Analysis of the muropeptide composition was performed essentially as described previously (Alvarez et al., 2020). Samples were treated with Proteinase K (20 µg/mL, 1 h, 37°C). The reaction was heat-inactivated and sacculi were further washed by ultracentrifugation. Finally, samples were digested overnight with muramidase (100 µg/mL) at 37°C. Muramidase digestion was stopped by boiling and coagulated proteins were removed by centrifugation (15 min, 14,000 rpm). For sample reduction, the pH of the supernatants was adjusted to pH 8.5–9.0 with sodium borate buffer and sodium borohydride was added to a final concentration of 10 mg/mL. After incubating for 30 min at room temperature, pH was adjusted to 3.5 with orthophosphoric acid. The soluble muropeptides were analysed by high-performance liquid chromatography (HPLC; Waters Corporation, USA) on a Kinetex C18 column (150 x 4.6 mm; 2.6 µm particle size, 100 Å) (Phenomenex, USA) and detected at 204 nm with UV detector (2489 UV/Visible, Waters Corporation, USA). Muropeptides were separated with organic buffers at 45°C using a linear gradient from buffer A (formic acid 0.1% (v/v) in water) to buffer B (formic acid 0.1% (v/v) in 40% acetonitrile) in a 18 minutes run with a 1 ml/min flow. Quantification of muropeptides was based on their relative abundances (relative area of the corresponding peak) normalized to their molar ratio. The molar percentage was calculated for each muropeptide. This relative molarity was also used to calculate the molar percentage of crosslinked muropeptides. Muropeptide identity was confirmed by MS analysis, using a Xevo G2-XS QTof system (Waters Corporation, USA).

FDAA incubations

For the sequential labelling of cells with HADA (7-hydroxycoumarin-3-carboxylic acid-D-alanine, blue), BADA (BODIPY FL-D-alanine; green) and TADA (TAMRA-D-alanine; red), exponential phase cells were pelleted, resuspended in medium containing the first label and then grown at 37°C. Specific media, incubation intervals and order of the labels for each *Neisseriaceae* species are listed in Table S2 and S3, respectively. After the first interval cells were washed twice with fresh medium (37°C) and centrifuged between washes (7,000 g for 2 min at RT). After this, the cell pellets were resuspended in pre-warmed medium containing label two. For triple labelling, cells were washed twice and resuspended in medium containing the third label. Cells were then immediately treated with 70% ice-cold ethanol and incubated on ice for 1 hour. Ethanol-fixed cells were collected via centrifugation (7,000 g for 2 minutes at RT), washed twice with 4°C 1 x Phosphate Buffered Saline (PBS, pH 7.4), resuspended in PBS, and stored on ice before imaging.

EDA-DA incubation and click-chemistry

To track symbiont cell wall growth followed by immunolabeling *Alysiella filiformis* cells were grown over night on PY plates. Single colonies were incubated in 10 mM ethynyl-D-alanyl-D-alanine (EDA-DA, a D-amino acid carrying a clickable ethynyl group) for 30 min, resuspended in pre-warmed PY medium, washed twice (7000 g for 2 minutes at RT) and treated with 70% ethanol like described before. After that, cells were rehydrated and washed in PBS containing 0.1% Tween 20 (PBT). Blocking was carried out for 30 min in PBS containing 0.1% Tween 20 (PBT) and 2% (wt/vol) bovine serum albumin (blocking solution) at room temperature. An Alexa488 fluorophore was covalently bound to EDA-DA via copper catalysed click-chemistry by following the user manual protocol for the Click-iT reaction cocktail (Click-iT EdU Imaging Kit, Invitrogen). The cells were incubated with the Click-iT reaction cocktail for 30 min at RT in the dark. Unbound dye was removed by a 10-min wash in PBT and one wash in PBS. For immunostaining of clicked bacterial cells, cells were washed for 10 min in PBT and subsequently incubated with blocking solution for 30 min at room temperature in the dark. From here on, immunostaining was performed as described below.

Western Blots

Proteins from bacteria cells were separated by reduced sodium dodecyl sulfate (SDS)-polyacrylamide gel electrophoresis (PAGE) on NuPAGE 4%–12% Bis-Tris pre-cast MOPS gel (Invitrogen), respectively, and each blotted onto Hybond ECL nitrocellulose membranes (Amersham Biosciences). Membranes were blocked for 45 min in PBS containing 5% (wt/vol) nonfat milk (PBSM) at room temperature and incubated overnight at 4°C with a 1:1,000 dilution of sheep polyclonal anti-*E. coli* K88 fimbrial protein AB/FaeG antibody (ab35292, Abcam) in PBSM. For the negative control, the primary antibody was

omitted. After five 6 min-long washes in PBSM and one final wash in PBS containing 0.1% Tween20, the blot was incubated for 1 h at room temperature with a horseradish peroxidase-conjugated anti-sheep secondary antibody (1:10,000; Amersham Biosciences) in PBSM. Protein-antibody complexes were visualized using ECL Plus detection reagents (Amersham Biosciences).

Immunostaining

Exponential phase cells were fixed overnight in 3% formaldehyde at 4°C. Cells were collected via centrifugation (7000 g for 2 minutes at RT), washed twice with PBS and resuspended in PBS containing 0.1 % Tween 20 (PBT). Blocking was carried out for 1 h in PBT containing 2% (wt/vol) bovine serum albumin (blocking solution) at room temperature. After that, cells were incubated with a 1:500 dilution of sheep polyclonal anti-*E. coli* K88 fimbrial protein AB/FaeG antibody (ab35292, Abcam) overnight at 4°C in blocking solution. Upon incubation with primary antibody (or without in the case of the negative control) samples were washed three times in PBT and incubated with an Alexa555 conjugated anti-sheep antibody (Thermo Fisher Scientific) at 1:500 dilution in blocking solution for 1 h at room temperature. Unbound secondary antibody was removed by two washing steps one in PBT and one in PBS. Cell pellets were resuspended in PBS containing 5 µg/mL Hoechst for 20 min and subsequently washed and resuspended with PBS. 1 µL of the bacterial solution was mixed with 0.5 µL of Vectashield mounting medium (Vector Labs) and mounted on an agarose slide.

Nile red membrane staining

Exponential phase cells were fixed overnight in 2 % formaldehyde at 4°C. Cells were collected via centrifugation (7000 g for 2 minutes at RT), washed twice with PBS and resuspended in PBS containing 10 µg/mL Nile Red (Stock is prepared with DMSO; ThermoFisher N1142) and 5 µg/mL Hoechst for 15 min in the dark at room temperature. Cells were washed and resuspended in PBS and subsequently 1 µL of the bacterial solution was mixed with 0.5 µL of Vectashield mounting medium (Vector Labs) and mounted on an agarose slide.

Fluorescence microscopy

For Figure 2 and Supplementary Figures S1 and S4 immunostained or FDAA-labelled bacteria were imaged using a Nikon Eclipse NI-U microscope equipped with a MFCool camera (Jenoptik) and images were acquired using the ProgRes Capture Pro 2.8.8 software (Jenoptik). For Figure 3 and Supplementary Figure S5, FDAA-labelled bacteria were visualized with a Leica TCS SP8 X confocal laser scanning microscope. Images were taken with a 63X Plan-Apochromat glycerine objective with a NA of 1.30 and a

refraction index of 1.46 (glass slide, glycerine and antifade mounting medium). The Leica software LASX (3.7.2.22383) was used for image acquisition and post-processing if necessary.

For Figure 6 and Supplementary Figure S8, FDAA-labelled *N. elongata* wild type (*rpsL**) and mutant (*rpsL**; *cdsA-amiC*$_{SM}$; *mreB*$_{SM}$) were imaged at the INRS-CAFSB platform with a Zeiss LSM 780 AxioObserver confocal microscope equipped with a Zeiss Plan-Apochromat 100x/1.4 Oil M27. The Zeiss software Zen 2011 was used for image acquisition.

FDAA fluorescence quantification and statistical analysis

Microscopic images were processed using the public domain program ImageJ (Schneider et al., 2012) in combination with plugin Fil-Tracer (this study). Cell outlines were traced and morphometric measurements recorded. Fluorescent intensities were measured along the septal plane and plotted as fraction of the normalized cell length. Automatic cell recognition was double-checked manually. For representative images, the background subtraction function of ImageJ was used and brightness and contrast were adjusted for better visibility. Data analysis was performed using Excel 2021 (Microsoft Corporation, USA), plots were created with ggplot2 in R (http://www.R-project.org/). Septa length (Figure 6 and S8) of BADA and TADA labelled cells were analysed using the public domain software Fiji (Schindelin et al., 2012). Cell and septa lengths were measured manually. Notably, only cells that showed a BADA and TADA signal were considered for the septa length measurements. Two-tailed unpaired T tests were performed using GraphPad Prism version 9.3.0 for Mac (La Jolla California USA, www.graphpad.com). Figures were compiled using Adobe Photoshop and Illustrator 2021 (Adobe Systems, USA).

Genome sequencing and assembly

Genomic DNA for WGS of *Neisseriaceae* species and PCR amplification of DNA used for cloning purposes or sequence verifications were extracted using Genomic Tip 20/G or 100/G kits (Qiagen) according to the manufacturer's instructions. The genome sequencing results are presented in Table S1. Genomes were sequenced either using a Pacific Biosciences RS II system at the Génome Québec Innovation Centre (McGill University, Montréal, Canada) or using Oxford Nanopore technologies at the Bacterial Symbiont Evolution Lab (INRS, Laval, Canada). For PacBio, the reads were assembled *de novo* using HGAP v.4 (Chin et al., 2013) available on SMRT Link v.7 (default parameters, except, min. subread length: 500; estimated genome size: 2.7 Mb). For nanopore sequencing, DNA libraries were prepared following the Native barcoding genomic DNA procedure (with EXP-NBD104, EXP-NBD114, and SQK-LSK109). The base call was carried out using guppy_basecaller (version 5.0.11+2b6dbff) in sup mode. Reads were filtered by quality Q> 8 and separated by barcodes using guppy_barcoder (version 5.0.11+2b6dbff). The genome assembly was made by 3 programs: Canu

(https://github.com/marbl/canu), Flye (https://github.com/fenderglass/Flye) (Koren et al., 2017) and Miniasm (https://github.com/lh3/miniasm) (Li, 2016). Then each ensemble was corrected in bases using Pilon (https://github.com/broadinstitute/pilon) (Walker et al., 2014). Racon (https://github.com/isovic/racon) (Vaser et al., 2017) Medaka (https://github.com/nanoporetech/medaka). All assemblies and assembly corrections were analysed with Quast (https://github.com/ablab/quast) (Gurevich et al., 2013) and BUSCO (https://gitlab.com/ezlab/busco) (Manni et al., 2021). The assembly with the least number of contigs and the greatest completeness was chosen.

Core-genome based phylogeny of *Neisseriaceae*

All genomes were annotated with Prokka v1.14.5 (Seemann, 2014). Core-genome genes were obtained by MAFFT alignment through Roary v3.11.2 (Page et al., 2015), considering a minimum percentage identity of 55 for blastp, and occurrence in at least 90% of the isolates. Best evolutionary model for each partition was found by IQ-TREE version 1.6.3 (Kalyaanamoorthy et al., 2017) and maximum-likelihood phylogenetic analysis was also performed using IQ-TREE (Nguyen et al., 2015) using 10,000 ultrafast bootstrap replicates (Hoang et al., 2018).

Genomic comparisons

For gene insertion and deletion, we have used the MycoHIT pipeline that was described before (Veyrier et al., 2009, 2011). We used complete genomes of all the rod-shaped and MuLDi *Neisseriaceae* species represented in Figure 1. We excluded the second coccus lineage (*Neisseria wadsworthii*, *Neisseria canis* and *N.* sp. 83E034). We performed an alignment search with the standalone TBLASTN program (Gerts et al., 2006), using the 2105 predicted proteins from *N. elongata* ATCC29315 or the 2349 predicted proteins from *S. muelleri* as the query sequences to search for matches in the genomic DNA of other organisms. We obtained two matrices of around 80000 scores (2063 or 2105 protein sequences blasted against 38 genomes) providing two types of output: categorical (hit versus no hit) and quantitative (degree of similarity). To categorically assign that there was no hit, we employed the default E-value of e-10. Thus, if the statistical significance ascribed to a comparison is greater than this E value, we assigned a percentage of similarity of 0% to that comparison. To analyse quantitative results, we used MycoHIT (Veyrier et al., 2009) to assign absence of gene in all MuLDi with presence of the gene in all rod-shape or vice versa. “Absence” was defined as lower values and “presence” as higher values, than the 95 percentile of tested species.

Study of a possible association between amino acid changes and their influence on cell shape was approached using CapriB (Guerra Maldonado JF, 2020). Briefly, two databases were generated considering *Simonsiella muelleri* ATCC 29453 (multicellular, accession number GCA_002951835.1) and

Neisseria elongata subs. glycolytica ATCC 29315 (bacilli, accession number GCA_000818035.1) as references. The proteins encoded in each genome under study here were further compared against these two references by TBLASTN. Once the blast results were obtained, and the groups to be compared were defined, i.e. multicellular versus bacilli, amino acid changes in proteins shared by both groups (identity threshold 60%) were investigated. In this regard, CapriB has several analysis options, but the study focused on those amino acids that remain identical in the members of one group but are modified in the other (I vs D option).

RNA sequencing and analysis

Total RNA was extracted from 6h cultures grown on GCB agar plates. The cells were harvested in RNA protect reagent (Qiagen). RNeasy Mini Kit (Qiagen) with RNase Free DNAse set (Qiagen) was used for RNA extraction according to the manufacturer's instructions.

The removal of ribosomal RNA for cDNA synthesis was done with NEBNext rRNA Depletion kit with 1 ug of total RNA in the purification using 1.8X Cytiva Sera-mag. For results presented in Figure 9, the rRNA depleted mRNA were processed using the Illumina® Stranded mRNA Prep protocol without modification by Génome Québec Innovation Centre (McGill University, Montréal, Canada). 100bp Pair-End Sequencing was performed with the NovaSeq 6000 system. Sequence reads were processed with FastQC (Version 0.73) to determine the quality before grooming by FastQ Groomer (Version 1.1.5). Paired FastQ reads were then aligned against *Neisseria elongata* subsp. glycolytica ATCC 29315 (accession number NZ_CP007726.1) genome using Bowtie2 (Version 2.4.2) and read counts were determined using htseq_count (Version 0.9.1) tool. Subsequently the gene expression of the transcripts was determined using DESeq2 (Version 2.22.40.6). Visualization of differentially expressed genes was done with Venn diagrams, drawn by a Web-based platform Venny 2.1 (https://bioinfogp.cnb.csic.es/tools/venny/).

For intra-genus transcriptomic comparison presented in Figure 8, rRNA depleted mRNA were treated using the RevertAid RT Reverse Transcription Kit (K1691; Thermo Scientific™) with some adjustments. For first strand cDNA synthesis, 1 ul of random primer (3 µg/µL ; 48190011; Invitrogen™) was added and the solution was incubated at 65°C. For the second strand cDNA synthesis, procedure was followed without RNA removal step and by purifying the double-stranded cDNA with 1.8X Cytiva Sera-mag. The cDNA were eluted in 24 µL of nuclease-free water. Libraries were prepared by PCR BARCODING (96) AMPLICONS (SQK-LSK109) and PCR BARCODING (SQK-PBK004) (Oxford Nanopore technologies), as described by the manufacturer. The base call was carried out using guppy_basecaller (version 5.0.11+2b6dbff) in sup mode, adapters were removed and filtered by quality Q> 8, they were separated by barcodes using guppy_barcoder (version 5.0.11+2b6dbff). In parallel, the ten indicated genomes were annotated with Prokka v1.14.5 (Seemann, 2014). Using each of the protein sequences (.faa) files, a standalone BLASTP (Camacho et al., 2009) was performed for each dyad possibility. Network connection was thereafter established with the python programming package NetworkX version 2.6.2 (Hagberg et al., 2008) with a cut-off of 60% of similarity. Basically, all proteins showing more than 60% similarities with

one of the members (putative homologues) were clustered together. Each cluster of proteins was named (example NEISS_1) and this name was used to replace the original locus-tags in the .GFF file (previously generated by Prokka). This was done using an homemade python script and has generated a new file that we called .GTF. This file was used to map the reads to the corresponding genomes using minimpa2 (Li, 2018). The .GTF and .sam files were used to perform the reads counts using featureCounts of Subread package (Liao et al., 2014). The count files for each sample were joined into a table using a homemade script and these results were analysed using DESeq2 version 3.14 (Love et al., 2014). Parameter used were Reads >1 in the 10 genomes (core-transcriptome: genes that were showing at least one read mapped in all genomes). We investigated the biological functions of the gene differentially expressed and the putative pathways that could link them through a STRING analysis (Szklarczyk et al., 2021).

Quantitative real-time PCR

RNA samples were standardized to a final concentration of 1 µg with addition of DNaseI Amplification grade (Invitrogen) for genomic DNA removal. Random primers (Invitrogen), and RevertAid H-Minus reverse transcriptase (Thermo Scientific) were used for complementary DNA synthesis (cDNA) according to the manufacturer's instructions. Absence of contaminating gDNA was verified by conventional PCR of RNA samples in the absence of reverse transcriptase. Gene expression of *dcw* cluster was verified by quantitative real-time PCR (qRT-PCR) using Power SYBR Green PCR master mix (Applied Biosystems) using primers listed in supplementary Table S2. Differential gene expression was calculated using ΔΔCT method using the mean CT value of each target, normalization was done relative to *gyrA* gene. Standard T-test using (GraphPad Prism v9.0; GraphPad Software, CA) was used to ascertain statistical significance of gene expression between the strains, where $P<0.05$ was considered significant.

AmiC and AmiC2 phylogeny

Sequences of N-acetylmuramoyl-alanine amidase from *S. muelleri* ATCC 29453 (AmiC, accession number AUX62143.1) and *C. kuhniae* (AmiC2, accession number WP_027009548.1) were searched by blastp against all the *Neisseriaceae* genomes included in this study, as well as the complete bacterial repertoire found at NCBI. Amino acid sequences of the hits obtained by blastp were retrieved from the entire set of genomes using faSomeRecords (https://github.com/santiagosnchez/faSomeRecords/blob/master/faSomeRecords.pl). The resulting sequences were aligned with MAFFT v7 (Katoh et al., 2002), and maximum-likelihood phylogenetic analysis was performed using IQ-TREE using 1,000 ultrafast bootstrap replicates.

Genomic organization of the *dcw* cluster and *cdsA* loci in the *Neisseriaceae*

Coordinates of the *dcw* cluster and of the *cdsA* loci were obtained by tblastn for each *Neisseriaceae* genome. Once the genomic location of each sequence was determined, the sequences were extracted using tools available in the EMBOSS package (Rice et al., 2000). The resulting sequences were annotated with Prokka, and the output gbk files were used to construct the synteny by employing EasyFig 2.2.2 (Sullivan et al., 2011).

Construction of mutant strains

Neisseria elongata mutant strains were done in *N. elongata* subsp. *glycolytica* (ATCC 29315) for single gene mutation and its streptomycin-resistant variant with a point mutations K88R *rpsL** for unmarked and multiple gene editing. *mraZ* was deleted by replacing *mraZ* with an mCherry-encoding gene. The construct for *mraZ* deletion was obtained by fusing multiple PCR fragments using Phusion DNA polymerase according to the protocol (New England Biolabs) as follows: firstly, *N. elongata* gDNA was used to amplify approximately 500 bp of regions up and down stream of *mraZ* using, respectively, primer pairs 5'KoMraZF-R and 3'KoMraZF-R. The promoter "pdcwSm", located upstream the *S. muelleri dcw* cluster, was amplified from *S. muelleri* gDNA using primer pairs pdcwsmF/pdcwsmR. Primer pairs 5MraZKmF and KmpSimR were used to amplify the kanamycin resistance cassette from pGEM::Km plasmid DNA (Veyrier et al., 2015), while the Mcherry cassette was obtained by PCR amplification of pMcherry10 (Addgene) using primer pairs pdcwsmMcherry F and McherryNsiIR. Subsequently, the 5'MraZ and Km cassette were fused using primer pairs 5KoMraZF and KmpSimR, while Mcherry and 3'MraZ were fused using primer pairs pdcwMcherryF and 3'KoMraZ R. Finally, 5'MraZ-KM, pdcwSm and Mcherry-3'MraZ fragments were fused using primer pairs 5KoMraZ F and 3KoMraZ R and the resulting DNA was used for transformation in *N. elongata*.

To overexpress *mraZ*, *Neisseria meningitidis* promoter, *porB* was amplified from *N. meningitis* gDNA using primer pairs (porBpF-porBpbluntR) while the *mraZ* gene was amplified from *N. elongata* gDNA using primer pairs (MraZSphIF-3MraZR). The *porB* promoter from *N. meningitis* and the mraZ gene from *N. elongata* were subsequently fused by PCR. This resulted in an approximately 1.6 kb-long porB:MraZ cassette that was digested using the restriction enzymes NheI and KpnI and then ligated with NheI-KpnI digested plasmid p5nrq3::Cm (Veyrier et al., 2015). The ligation mix was transformed in *E. coli* DH5α cells to obtain the porBMraZ::p5nrq3::Cm plasmid. The plasmid was subsequently linearized before transformation into the *Neisseria elongata DmraZ* strain.

For the single knockout of *ΔmraZ*, Δ*rapZ*, Δ*gloB* or Δ*dgt*, we used a cassette developed in our laboratory named RPLK (Nyongesa et al., n.d. submitted) that contains the wild-type *N. elongata rpsL* gene, *N. meningitidis* promoter *porBp,* the blue-white screening selection marker *lacZ* and the kanamycin resistance marker that facilitated the generation of unmarked deletion in addition to multiple gene editing. We used synthesized DNAs (BioBasic) that contain approximately 500 bp each 5' and 3' regions surrounding the respective genes with a central BglII restriction site and cloned into pUC57 plasmid. The plasmids were linearized using BglII and ligated with RPLK cassette (Nyongesa et al., n.d. submitted).

Mutants were obtained by transforming either *N. elongata* wild-type (single KO) or an *N. elongata* streptomycin-resistant strain (indicated *rpsL**) (multiple KO) with the linearized plasmid of the targeted gene that resulted in blue, kanamycin-resistant, streptomycin sensitive clones. Markerless deletion was achieved by introducing DNA of the 5'-3' homologous regions of the target gene thereby excising the RPLK cassette resulting in white, kanamycin sensitive and streptomycin resistant clones. Subsequent genes of interest were edited by repeating this procedure and verifications of the correct excision was done by PCR.

For allelic switching of *N. elongata mreB* with that from *S. muelleri*, plasmid pMreBSimon-3'RD3Ne was obtained by amplifying *S. muelleri* mreB using primer pairs MreBsimonF – MreBsimonR, while the subsequent region of the locus (3'RD3Ne that comprise a piece of *mreCD*) was amplified from *N. elongata* using primer pairs 3'RD3NeF-3'RD3NeR. The two products were fused using primer pairs MreBsimonF - 3'RD3NeR. This generated a cassette of $mreB_{sm}$ fused with $mreCD_{ne}$ that was then digested by restriction enzymes BamHI and SpeI before ligation with plasmid p5KORD1Ne::cm (Veyrier et al., 2015) digested with the same enzymes to obtain plasmid pMreBsimon3'RD3Ne::cm. The plasmid was linearized with ScaI before transformation in *N. elongata* strains. $mreB_{sm}$ positive and $mreB_{ne}$ negative clones were confirmed by PCR.

For the *cdsA-amiC2* knock-in constructs, we used the plasmid pUCNe ::ampR that contains 5' and 3' *Neisseria elongata* homologous regions to the intergenic locus between two genes coding for hypothetical proteins at position 888015 (insertion site). We first constructed the pUCNe::RPLK plasmid by ligating the RPLK cassette using BglII. Secondly, *cdsA-AmiC2* PCR product was obtained using primer pairs cdsAmiC2F-amiC2R, was digested using BglI and ligated to pUCNe::ampR to produce the pUCcdsamiC2::ampR plasmid. The mutants were obtained with a two-step methods (Nyongesa et al., n.d. submitted). First, we transformed the plasmid pUCNe::RPLK into *N. elongata rpsl** to obtain N. elongata RPLK (RPLK inserted at position 888015). In the second step, we have replaced the RPLK cassette with *cdsA-amiC2* genes, by transforming the pUCcdsamiC2::ampR plasmid linearized using ScaI into *N. elongata* RPLK. *cdsamic2* positive transformants were confirmed by PCR.

Data and code availability. The documentation for the ImageJ plugin Fil-Tracer can be accessed here: https://sils.fnwi.uva.nl/bcb/objectj/examples/Fil-Tracer/MD/Fil-Tracer.html

Declarations

AUTHOR CONTRIBUTIONS

S.N. and P.M.W did most experiments, visualization and formal analysis, wrote and revised the manuscript. E.B.; F.P; M.N.; M.D; C.N.; T.V.; N.K.; A.R.M. and A.N. did some experiments and formal analysis and critically revised the manuscript. N.O.E.V. contributed ImageJ analysis tools (ObjectJ, Fil-Tracer). M.V. contributed materials. Y.B. acquired funding and analysis tools. F.C. acquired funding, did

formal analysis and revised manuscript. S.B. conceptualized and supervised the work, acquired funding, provided resources, wrote and revised the manuscript. F.J.V. did experiments, formal analysis, conceptualized and supervised the work, acquired funding, provided resources, wrote and revised the manuscript.

FUNDING

This work was supported by the Natural Sciences and Engineering Research Council of Canada (NSERC) discovery grant (RGPIN-2016-04940) (F.V.), the Fonds De Recherche du Quebec Nature et technologies (FRQNT) Établissement de la relève professorale (205027) (F.V.) and the Austrian Science Fund (FWF) project P28593-B22 (S.B., P.M.W., T.V., N.K.). P.M.W. also received DOC-fellowship 25240 from the Austrian Academy of Science and a PhD completion grant from the University of Vienna. E.B. received a Ph.D. Fellowship from the Fondation Armand-Frappier. M.D. was partially supported by a postdoctoral fellowship from the Swiss National Science Foundation (project #P2GEP3_191489). C.N. Received a Ph.D. studentship Calmette & Yersin from the Institut Pasteur International Network. Research in the Cava lab was supported by The Swedish Research Council (VR), The Knut and Alice Wallenberg Foundation (KAW), The Laboratory of Molecular Infection Medicine Sweden (MIMS), and The Kempe Foundation. M.N. was funded by a postdoctoral fellowship from the Swedish Society for Medical Research (SSMF). Y.V.B. is also supported by a Canada 150 Research Chair in Bacterial Cell Biology. F.J.V. received a Junior 1 and Junior 2 research scholar salary award from the Fonds de Recherche du Québec - Santé. The funders had no role in study design, data collection and analysis, decision to publish, or preparation of the manuscript.

ACKNOWLEDGEMENTS

The authors are extremely grateful to Markus Christian Schmid and the Division of Microbial Ecology of the University of Vienna for providing the confocal microscope and technical support with the imaging. P.M.W. is grateful to B. Bejtovic for preliminary experiments. We thank Nathan Weyand for providing us *N.* sp. DentCa1247. We thank Tanneke den Blaauwen of the University of Amsterdam for inspiring and constructive discussions.

DECLARATION OF INTEREST

The authors declare no competing interests.

References

Addinall, S.G., Lutkenhaus, J., 1996. FtsZ-spirals and -arcs determine the shape of the invaginating septa in some mutants of Escherichia coli. Mol. Microbiol. 22, 231–237.

Adeolu, M., Gupta, R.S., 2013. Phylogenomics and molecular signatures for the order Neisseriales: Proposal for division of the order Neisseriales into the emended family Neisseriaceae and Chromobacteriaceae fam. nov. Antonie van Leeuwenhoek, Int. J. Gen. Mol. Microbiol. 104, 1–24.

Altschul, S.F., Madden, T.L., Schäffer, A.A., Zhang, J., Zhang, Z., Miller, W., Lipman, D.J., 1997. Gapped BLAST and PSI-BLAST: a new generation of protein database search programs. Nucleic Acids Res. 25, 3389–3402.

Alvarez, L., Cordier, B., van Teeffelen, S., Cava, F., 2020. Analysis of Gram-negative Bacteria Peptidoglycan by Ultra-performance Liquid Chromatography. BIO-PROTOCOL 10.

Ayala, J.A., Garrido, T., De Pedro, M.A., Vicente, M., 1994. Chapter 5 Molecular biology of bacterial septation. New Compr. Biochem. 27, 73–101.

Bi, E., Lutkenhaus, J., 1991. FtsZ ring structure associated with division in Escherichia coli. Nature 354, 161–164.

Bisson-Filho, A.W., Hsu, Y.-P., Squyres, G.R., Kuru, E., Wu, F., Jukes, C., Sun, Y., Dekker, C., Holden, S., VanNieuwenhze, M.S., Brun, Y. V, Garner, E.C., 2017. Treadmilling by FtsZ filaments drives peptidoglycan synthesis and bacterial cell division. Science (80-.). 355, 739 LP – 743.

Brennan, C.A., Garrett, W.S., 2018. Fusobacterium nucleatum — symbiont, opportunist and oncobacterium. Nat. Rev. Microbiol. 2018 173 17, 156–166.

Bulgheresi, S., 2016. Bacterial cell biology outside the streetlight. Environ. Microbiol. 18, 2305–2318.

Busiek, K.K., Margolin, W., 2015. Bacterial actin and tubulin homologs in cell growth and division. Curr. Biol. 25, R243–R254.

Buskermolen, J.K., Reijnders, C.M.A., Spiekstra, S.W., Steinberg, T., Kleverlaan, C.J., Feilzer, A.J., Bakker, A.D., Gibbs, S., 2016. Development of a Full-Thickness Human Gingiva Equivalent Constructed from Immortalized Keratinocytes and Fibroblasts. Tissue Eng. - Part C Methods 22, 781–791.

Camacho, C., Coulouris, G., Avagyan, V., Ma, N., Papadopoulos, J., Bealer, K., Madden, T.L., 2009. BLAST+: Architecture and applications. BMC Bioinformatics 10, 1–9.

Chen, S., Rudra, B., Gupta, R.S., 2021. Phylogenomics and molecular signatures support division of the order Neisseriales into emended families Neisseriaceae and Chromobacteriaceae and three new families Aquaspirillaceae fam. nov., Chitinibacteraceae fam. nov., and Leeiaceae fam. nov. Syst. Appl. Microbiol. 44, 126251.

Chin, C.S., Alexander, D.H., Marks, P., Klammer, A.A., Drake, J., Heiner, C., Clum, A., Copeland, A., Huddleston, J., Eichler, E.E., Turner, S.W., Korlach, J., 2013. Nonhybrid, finished microbial genome assemblies from long-read SMRT sequencing data. Nat. Methods 10, 563–569.

Claessen, D., Rozen, D.E., Kuipers, O.P., Søgaard-Andersen, L., van Wezel, G.P., 2014. Bacterial solutions to multicellularity: a tale of biofilms, filaments and fruiting bodies. Nat. Rev. Microbiol. 2014 122 12, 115–124.

den Blaauwen, T., 2018. Is longitudinal division in rod-shaped bacteria a matter of swapping axis? Front. Microbiol. 9, 822.

Du, S., Lutkenhaus, J., 2019. At the Heart of Bacterial Cytokinesis: The Z Ring. Trends Microbiol. 27, 781–791.

Dudek, N.K., Galaz-Montoya, J.G., Shi, H., Mayer, M., Danita, C., Celis, A.I., Wu, G.-H., Behr, B., Huang, K.C., Chiu, W., Relman, D.A., 2021. Previously uncharacterized rectangular bacteria in the dolphin mouth. bioRxiv 2021.10.23.465578.

Eraso, J.M., Markillie, L.M., Mitchell, H.D., Taylor, R.C., Orr, G., Margolin, W., 2014. The highly conserved MraZ protein is a transcriptional regulator in Escherichia coli. J. Bacteriol. 196, 2053–2066.

Ericsson, A.C., Hagan, C.E., Davis, D.J., Franklin, C.L., 2014. Segmented filamentous bacteria: Commensal microbes with potential effects on research. Comp. Med. 64, 90–98.

Fisunov, G.Y., Evsyutina, D. V, Semashko, T.A., Arzamasov, A.A., Manuvera, V.A., Letarov, A. V, Govorun, V.M., 2016. Binding site of MraZ transcription factor in Mollicutes. Biochimie 125, 59–65.

Flores, E., Nieves-Morión, M., Mullineaux, C.W., 2019. Cyanobacterial septal junctions: Properties and regulation. Life 9.

Gerts, E.M., Yu, Y.K., Agarwala, R., Schäffer, A.A., Altschul, S.F., 2006. Composition-based statistics and translated nucleotide searches: Improving the TBLASTN module of BLAST. BMC Biol. 4, 1–14.

Guerra Maldonado, J.F., Vincent, A.T., Chenal, M., Veyrier, F.J., 2020. CAPRIB: a user-friendly tool to study amino acid changes and selection for the exploration of intra-genus evolution. BMC Genomics 21, 1–14.

Gurevich, A., Saveliev, V., Vyahhi, N., Tesler, G., 2013. QUAST: Quality assessment tool for genome assemblies. Bioinformatics 29, 1072–1075.

Hagberg, A., Swart, P., S Chult, D., 2008. Exploring network structure, dynamics, and function using NetworkX.

Hampton, J.C., Rosario, B., 1965. The attachment of microorganisms to epithelial cells in the distal ileum of the mouse. Lab. Investig. 14, 1464–1481.

Hedlund, B.P., Kuhn, D.A., 2006. The Genera Simonsiella and Alysiella. The Prokaryotes, 5, 828–839.

Hedlund, B.P., Tønjum, T., 2015. Simonsiella. Bergey's Man. Syst. Archaea Bact. 1–12.

Hoang, D.T., Chernomor, O., Von Haeseler, A., Minh, B.Q., Vinh, L.S., 2018. UFBoot2: Improving the ultrafast bootstrap approximation. Mol. Biol. Evol. 35.

Höltje, J.-V., 1998. Growth of the Stress-Bearing and Shape-Maintaining Murein Sacculus of Escherichia coli . Microbiol. Mol. Biol. Rev. 62, 181–203.

Jonsson, H., Hugerth, L.W., Sundh, J., Lundin, E., Andersson, A.F., 2020. Genome sequence of segmented filamentous bacteria present in the human intestine. Commun. Biol. 3, 1–9.

Kaiser, G. E., Starzyk, M.J., 1973. Ultrastructure and cell division of an oral bacterium resembling Alysiella filiformis. Can. J. Microbiol. 19, 325–327.

Kaiser, Gary E, Starzyk, M.J., 1973. Ultrastructure and cell division of an oral bacterium resembling Alysiella filiformis. Can. J. Microbiol. 19, 325–327.

Kalyaanamoorthy, S., Minh, B.Q., Wong, T.K.F., Von Haeseler, A., Jermiin, L.S., 2017. ModelFinder: Fast model selection for accurate phylogenetic estimates. Nat. Methods 14.

Katoh, K., Misawa, K., Kuma, K.I., Miyata, T., 2002. MAFFT: A novel method for rapid multiple sequence alignment based on fast Fourier transform. Nucleic Acids Res. 30, 3059–3066.

Kawazura, T., Matsumoto, K., Kojima, K., Kato, F., Kanai, T., Niki, H., Shiomi, D., 2017. Exclusion of assembled MreB by anionic phospholipids at cell poles confers cell polarity for bidirectional growth. Mol. Microbiol. 104, 472–486.

Khan, M.A., Durica-Mitic, S., Göpel, Y., Heermann, R., Görke, B., 2020. Small RNA-binding protein RapZ mediates cell envelope precursor sensing and signaling in Escherichia coli. EMBO J. 39, e103848.

Kieft, T.L., Simmons, K.A., 2015. Allometry of animal-microbe interactions and global census of animal-associated microbes. Proc. R. Soc. B Biol. Sci. 282.

Koren, S., Walenz, B.P., Berlin, K., Miller, J.R., Bergman, N.H., Phillippy, A.M., 2017. Canu: Scalable and accurate long-read assembly via adaptive κ-mer weighting and repeat separation. Genome Res. 27, 722–736.

Kosten, I.J., Buskermolen, J.K., Spiekstra, S.W., De Gruijl, T.D., Gibbs, S., 2015. Gingiva Equivalents Secrete Negligible Amounts of Key Chemokines Involved in Langerhans Cell Migration Compared to Skin Equivalents. J. Immunol. Res. 2015.

Kuhn, D.A., Gregory, D.A., Buchanan, G.E., Nyby, M.D., Daly, K.R., 1978. Isolation, characterization, and numerical taxonomy of Simonsiella strains from the oral cavities of cats, dogs, sheep, and humans. Arch.

Microbiol. 118, 235–241.

Leisch, N., Pende, N., Weber, P.M., Gruber-Vodicka, H.R., Verheul, J., Vischer, N.O.E., Abby, S.S., Geier, B., den Blaauwen, T., Bulgheresi, S., 2016. Asynchronous division by non-ring FtsZ in the gammaproteobacterial symbiont of *Robbea hypermnestra*. Nat. Microbiol. 2, 16182.

Leisch, N., Verheul, J., Heindl, N.R., Gruber-Vodicka, H.R., Pende, N., Den Blaauwen, T., Bulgheresi, S., 2012. Growth in width and FtsZ ring longitudinal positioning in a gammaproteobacterial symbiont. Curr. Biol. 22, R831–R832.

Li, H., 2018. Minimap2: Pairwise alignment for nucleotide sequences. Bioinformatics 34, 3094–3100.

Li, H., 2016. Minimap and miniasm: Fast mapping and de novo assembly for noisy long sequences. Bioinformatics 32, 2103–2110.

Liao, Y., Smyth, G.K., Shi, W., 2014. featureCounts: an efficient general purpose program for assigning sequence reads to genomic features. Bioinformatics 30, 923–930.

Love, M.I., Huber, W., Anders, S., 2014. Moderated estimation of fold change and dispersion for RNA-seq data with DESeq2. Genome Biol. 15, 1–21.

Manni, M., Berkeley, M.R., Seppey, M., Simão, F.A., Zdobnov, E.M., 2021. BUSCO Update: Novel and Streamlined Workflows along with Broader and Deeper Phylogenetic Coverage for Scoring of Eukaryotic, Prokaryotic, and Viral Genomes. Mol. Biol. Evol. 38, 4647–4654.

Mark Welch, J.L., Ramírez-Puebla, S.T., Borisy, G.G., 2020. Oral Microbiome Geography: Micron-Scale Habitat and Niche. Cell Host Microbe 28, 160–168.

Martínez-Torró, C., Torres-Puig, S., Marcos-Silva, M., Huguet-Ramón, M., Muñoz-Navarro, C., Lluch-Senar, M., Serrano, L., Querol, E., Piñol, J., Pich, O.Q., 2021. Functional Characterization of the Cell Division Gene Cluster of the Wall-less Bacterium Mycoplasma genitalium. Front. Microbiol. 12, 695572.

Mengin-Lecreulx, D., Ayala, J., Bouhss, A., Van Heijenoort, J., Parquet, C., Hara, H., 1998. Contribution of the P(mra) promoter to expression of genes in the Escherichia coli mra cluster of cell envelope biosynthesis and cell division genes. J. Bacteriol. 180, 4406–4412.

Mingorance, J., Tamames, J., Vicente, M., 2004. Genomic channeling in bacterial cell division. J. Mol. Recognit. 17, 481–487.

Monahan, L.G., Robinson, A., Harry, E.J., 2009. Lateral FtsZ association and the assembly of the cytokinetic Z ring in bacteria. Mol. Microbiol. 74, 1004–1017.

Monds, R.D., O'Toole, G.A., 2009. The developmental model of microbial biofilms: ten years of a paradigm up for review. Trends Microbiol. 17, 73–87.

Murray, R.G., Steed, P., Elson, H.E., 1965. The Location of the Mucopeptide in Sections of the Cell Wall of Escherichia Coli and Other Gram-Negative Bacteria. Can. J. Microbiol. 11, 547–560.

Nguyen, L.T., Schmidt, H.A., Von Haeseler, A., Minh, B.Q., 2015. IQ-TREE: A fast and effective stochastic algorithm for estimating maximum-likelihood phylogenies. Mol. Biol. Evol. 32, 268–274.

Nikolaichik, Y.A., Donachie, W.D., 2000. Conservation of gene order amongst cell wall and cell division genes in Eubacteria, and ribosomal genes in Eubacteria and Eukaryotic organelles. Genetica 108, 1–7.

Nyongesa, S., Chenal, M., Bernet, E., Coudray, F., Veyrier, F.J., n.d. Sequential markerless genetic manipulations of species from the Neisseria genus. submitted.

Page, A.J., Cummins, C.A., Hunt, M., Wong, V.K., Reuter, S., Holden, M.T.G., Fookes, M., Falush, D., Keane, J.A., Parkhill, J., 2015. Roary: Rapid large-scale prokaryote pan genome analysis. Bioinformatics 31, 3691–3693.

Pangborn, J., Kuhn, D.A., Woods, J.R., 1977. Dorsal-ventral differentiation in Simonsiella and other aspects of its morphology and ultrastructure. Arch. Microbiol. 1977 1133 113, 197–204.

Pende, N., Wang, J., Weber, P.M., Verheul, J., Kuru, E., Rittmann, S.K.M.R., Leisch, N., VanNieuwenhze, M.S., Brun, Y. V., den Blaauwen, T., Bulgheresi, S., 2018. Host-Polarized Cell Growth in Animal Symbionts. Curr. Biol. 28, 1039-1051.e5.

Ramond, E., Maclachlan, C., Clerc-Rosset, S., Knott, G.W., Lemaitre, B., 2016. Cell division by longitudinal scission in the insect endosymbiont Spiroplasma poulsonii. MBio 7, 1–5.

Rice, P., Longden, L., Bleasby, A., 2000. EMBOSS: the European Molecular Biology Open Software Suite. Trends Genet. 16, 276–277.

Schindelin, J., Arganda-Carreras, I., Frise, E., Kaynig, V., Longair, M., Pietzsch, T., Preibisch, S., Rueden, C., Saalfeld, S., Schmid, B., Tinevez, J.Y., White, D.J., Hartenstein, V., Eliceiri, K., Tomancak, P., Cardona, A., 2012. Fiji: An open-source platform for biological-image analysis. Nat. Methods. https://doi.org/10.1038/nmeth.2019

Schneider, C.A., Rasband, W.S., Eliceiri, K.W., 2012. NIH Image to ImageJ: 25 years of image analysis. Nat. Methods. https://doi.org/10.1038/nmeth.2089

Schnupf, P., Gaboriau-Routhiau, V., Gros, M., Friedman, R., Moya-Nilges, M., Nigro, G., Cerf-Bensussan, N., Sansonetti, P.J., 2015. Growth and host interaction of mouse segmented filamentous bacteria in vitro. Nature 520, 99–103.

Schnupf, P., Gaboriau-Routhiau, V., Sansonetti, P.J., Cerf-Bensussan, N., 2017. Segmented filamentous bacteria, Th17 inducers and helpers in a hostile world. Curr. Opin. Microbiol. 35, 100–109.

Seemann, T., 2014. Prokka: Rapid prokaryotic genome annotation. Bioinformatics 30.

Sen, B.C., Wasserstrom, S., Findlay, K., Söderholm, N., Sandblad, L., von Wachenfeldt, C., Flärdh, K., 2019. Specific amino acid substitutions in β strand S2 of FtsZ cause spiraling septation and impair assembly cooperativity in Streptomyces spp. Mol. Microbiol. 112, 184–198.

Shi, H., Bratton, B.P., Gitai, Z., Huang, K.C., 2018. How to Build a Bacterial Cell: MreB as the Foreman of E. coli Construction. Cell 172, 1294–1305.

Shi, H., Colavin, A., Bigos, M., Tropini, C., Monds, R.D., Huang, K.C., 2017. Deep Phenotypic Mapping of Bacterial Cytoskeletal Mutants Reveals Physiological Robustness to Cell Size. Curr. Biol. 27, 3419-3429.e4.

Siefert, J.L., Fox, G.E., 1998. Phylogenetic mapping of bacterial morphology. Microbiology 144, 2803–2808.

Sullivan, M.J., Petty, N.K., Beatson, S.A., 2011. Easyfig: A genome comparison visualizer. Bioinformatics 27, 1009–1010.

Szklarczyk, D., Gable, A.L., Nastou, K.C., Lyon, D., Kirsch, R., Pyysalo, S., Doncheva, N.T., Legeay, M., Fang, T., Bork, P., Jensen, L.J., von Mering, C., 2021. The STRING database in 2021: Customizable protein-protein networks, and functional characterization of user-uploaded gene/measurement sets. Nucleic Acids Res. 49, D605–D612.

Szwedziak, P., Löwe, J., 2013. Do the divisome and elongasome share a common evolutionary past? Curr. Opin. Microbiol. 16, 745–751.

Tamames, J., González-Moreno, M., Mingorance, J., Valencia, A., Vicente, M., 2001. Bringing gene order into bacterial shape. Trends Genet. 17, 124–126.

Thanbichler, M., 2018. Cell Division: Symbiotic Bacteria Turn It Upside Down. Curr. Biol. 28, R306–R308.

Vaser, R., Sović, I., Nagarajan, N., Šikić, M., 2017. Fast and accurate de novo genome assembly from long uncorrected reads. Genome Res. 27, 737–746.

Veyrier, F., Pletzer, D., Turenne, C., Behr, M.A., 2009. Phylogenetic detection of horizontal gene transfer during the step-wise genesis of Mycobacterium tuberculosis. BMC Evol. Biol. 9.

Veyrier, F.J., Biais, N., Morales, P., Belkacem, N., Guilhen, C., Ranjeva, S., Sismeiro, O., Péhau-Arnaudet, G., Rocha, E.P., Werts, C., Taha, M.K., Boneca, I.G., 2015. Common Cell Shape Evolution of Two Nasopharyngeal Pathogens. PLoS Genet. 11, 1–23.

Veyrier, F.J., Dufort, A., Behr, M.A., 2011. The rise and fall of the Mycobacterium tuberculosis genome. Trends Microbiol. 19, 156–161.

Vicente, M., Gomez, M.J., Ayala, J.A., 1998. Regulation of transcription of cell division genes in the Eschericia coli dcw cluster. Cell. Mol. Life Sci. 54, 317–324.

Walker, B.J., Abeel, T., Shea, T., Priest, M., Abouelliel, A., Sakthikumar, S., Cuomo, C.A., Zeng, Q., Wortman, J., Young, S.K., Earl, A.M., 2014. Pilon: An integrated tool for comprehensive microbial variant detection and genome assembly improvement. PLoS One 9, e112963.

Whitman, W.B., Coleman, D.C., Wiebe, W.J., 1998. Prokaryotes: The unseen majority. Proc. Natl. Acad. Sci. U. S. A. 95, 6578–6583.

Xiao, X., Willemse, J., Voskamp, P., Li, X., Prota, A.E., Lamers, M., Pannu, N., Abrahams, J.P., Van Wezel, G.P., 2021. Ectopic positioning of the cell division plane is associated with single amino acid substitutions in the FtsZ-recruiting SsgB in Streptomyces. Open Biol. 11.

Xie, C.H., Yokota, A., 2005. Phylogenetic analysis of Alysiella and related genera of Neisseriaceae: Proposal of Alysiella crassa comb. nov., Conchiformibium steedae gen. nov., comb. nov., Conchiformibium kuhniae sp. nov. and Bergeriella denitrificans gen. nov., comb. nov. J. Gen. Appl. Microbiol. 51, 1–10.

Yang, X., Lyu, Z., Miguel, A., McQuillen, R., Huang, K.C., Xiao, J., 2017. GTPase activity–coupled treadmilling of the bacterial tubulin FtsZ organizes septal cell wall synthesis. Science (80-.). 355, 744 LP – 747.

Young, K.D., 2006. The Selective Value of Bacterial Shape. Microbiol. Mol. Biol. Rev. 70, 660–703.

Zhang, L., Willemse, J., Claessen, D., Van Wezel, G.P., 2016. SepG coordinates sporulation-specific cell division and nucleoid organization in Streptomyces coelicolor. Open Biol. 6.

Figures

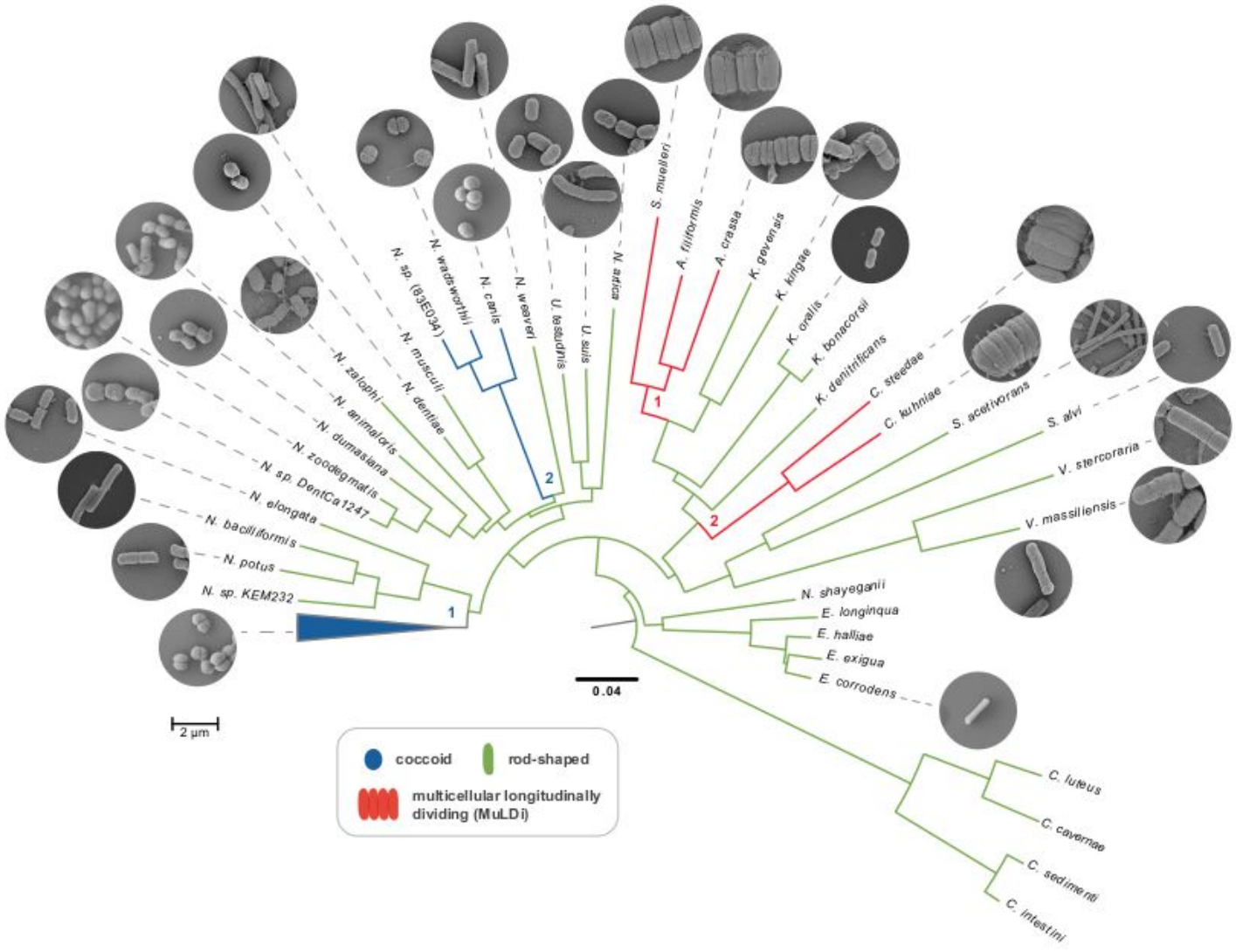

Figure 1

Core genome-based phylogeny of rod-shaped, coccoid and MuLDi *Neisseriaceae*. The best evolutionary model for each partition was found by IQ-TREE version 1.6.3 (Kalyaanamoorthy et al., 2017) and maximum-likelihood phylogenetic analysis was also performed using IQ-TREE (Nguyen et al., 2015) using 10,000 ultrafast bootstrap replicates (Hoang et al., 2018). Above the name of each species, scanning electron microscopy images display their morphology. Dark and light blue: coccoid *Neisseriaceae*; green: rod-shaped *Neisseriaceae*; red: multicellular longitudinally dividing (MuLDi) *Neisseriaceae*. Coccoid lineages 1 and 2 are indicated in blue. MuLDi lineages 1 and 2 are indicated in red. N.: *Neisseria*; U.: *Uruburella*; S.: *Simonsiella*; A.: *Alysiella*; K.: *Kingella*; C.: *Conchiformibius*; S.: *Snodgrassella*; V.: *Vitreoscilla*; E.: *Eikenella*; C.: *Crenobacter*. *Crenobacter* spp. (*Chromobacteriaceae*) serve as out-group.

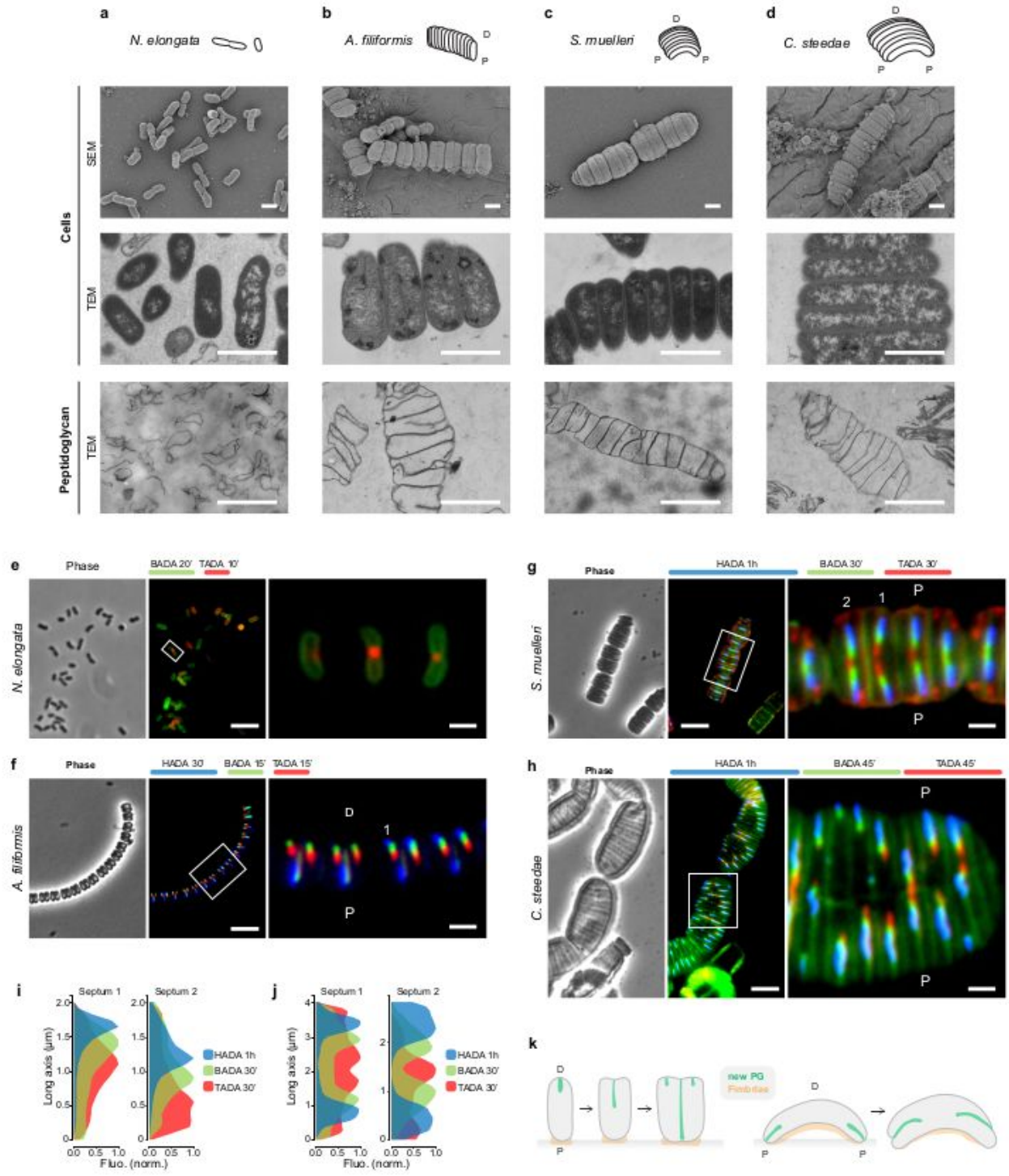

Figure 2

Morphology and epifluorescence microscope-based PG insertion pattern in four oral cavity symbionts belonging to the *Neisseriaceae*. (a-d) Schematic representations and electron microscope images (left to right) of (a) *N. elongata*, (b) *A. filiformis*, (c) *S. muelleri* and (d) *C. steedae*. P: proximal (host-attached) region of the cell. D: distal region of the cell. Scale bars correspond to 1 µm. (e-f) Phase contrast images (left panels), corresponding epifluorescence images (middle panels) and higher magnification images of selected regions (white frames; right panels). (e) *N. elongata* was incubated for 20 min with BADA (green)

and, subsequently, for 10 min in TADA (red). (f) *A. filiformis* was labelled consecutively with HADA, BADA and TADA for 30 min, 15 min and 15 min, respectively. (g) *S. muelleri* was labelled with HADA, BADA and TADA for 1 h, 30 min and 30 min, respectively. (h) *C. steedae* was labelled with HADA, BADA and TADA for 1 h, 45 min and 45 min, respectively. Septal fluorescence of HADA, BADA and TADA was plotted onto the long axis for two representative *A. filiformis* cells (i) and *S. muelleri* (j). Scale bars are 5 μm (middle panels) and 1 μm (right panels). (k) Schematic representation of *A. filiformis* (left), and *S. muelleri* or *C. steedae* (right) growth modes.

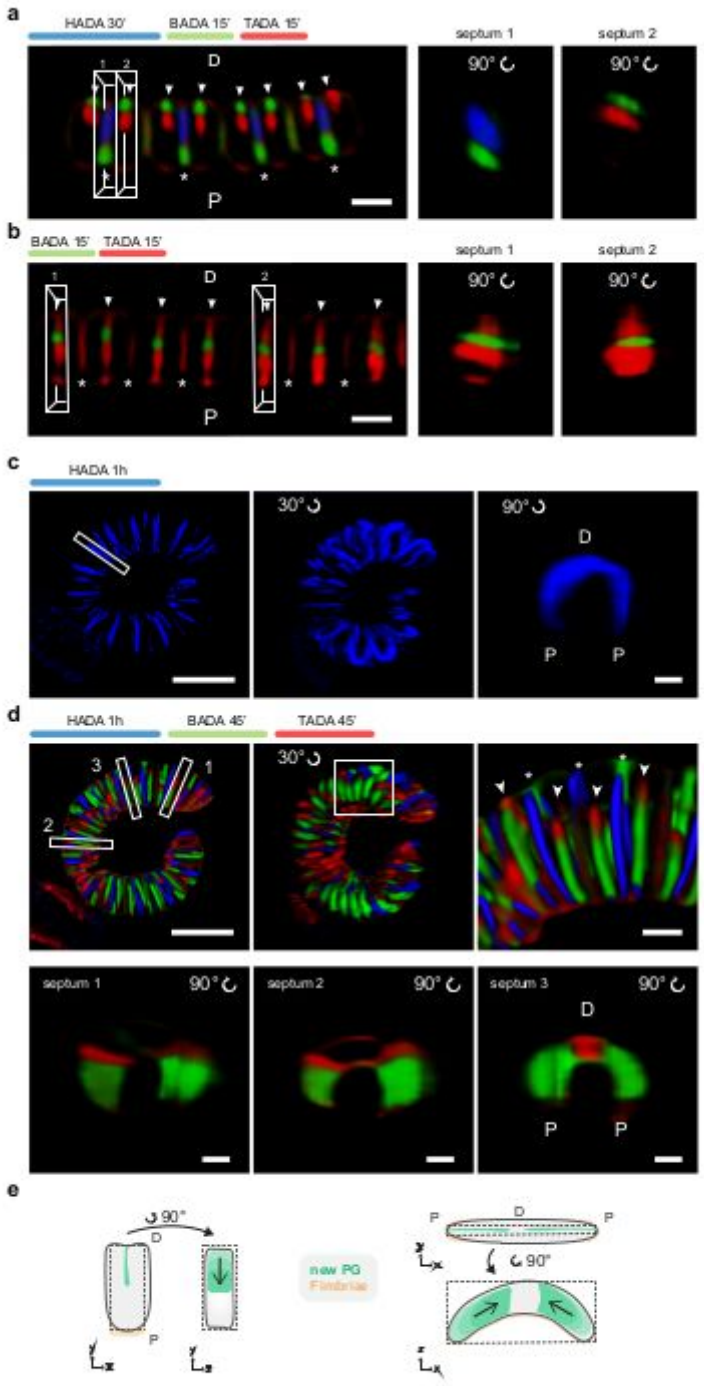

Figure 3

Confocal microscopy-based PG insertion pattern in *Alysiella filiformis* and *Conchiformibius steedae*. (a and b) *A. filiformis* was labelled consecutively with HADA, BADA and TADA for 30 min, 15 min and 15 min, respectively. (a) Left panel shows the front view of a filament. The distal (D) and proximal (P) poles are indicated. Stars point at newly completed septa, arrowheads point at incoming septa. Fluorescence emitted by a newly completed septum (septum 1 in white box) and by an incoming septum (septum 2 in

white box) were rotated by 90° and are displayed in the middle and the right panels, respectively. (b) Left most panel shows the front view of a second filament. Septa of cells undergoing two subsequent septation stages (septa 1 and 2 in white boxes) were rotated by 90° and are displayed in the two rightmost panels. The HADA signal is not visible. Scale bars are 1 µm. (c and d) *C. steedae* was labelled with HADA, BADA and TADA for 1 h, 45 min and 45 min, respectively. (c) Lateral view of the HADA fluorescence emitted by a filament (left panel). The same filament was rotated by 30° (middle panel) and the septum of one cell (white frame) was rotated by 90° (right panel). Scale bars are 5 µm (left and middle panel) and 1 µm (right panel). (d) Top panels: HADA, BADA and TADA fluorescence of the filament displayed in c (left and middle panels). Higher magnification of a region of interest indicated by a white frame (right panel). Bottom panels: three septa at consecutive septation stages (septa 1-3 in white frames) were rotated by 90° and ordered from the earliest to the latest. The distal (D) and proximal (P) cell poles are indicated. Scale bars are 5 µm (left upper corner) and 1 µm. (e) Schematic representation of *A. filiformis* (left) and *S. muelleri* or *C. steedae* (right) septation modes.

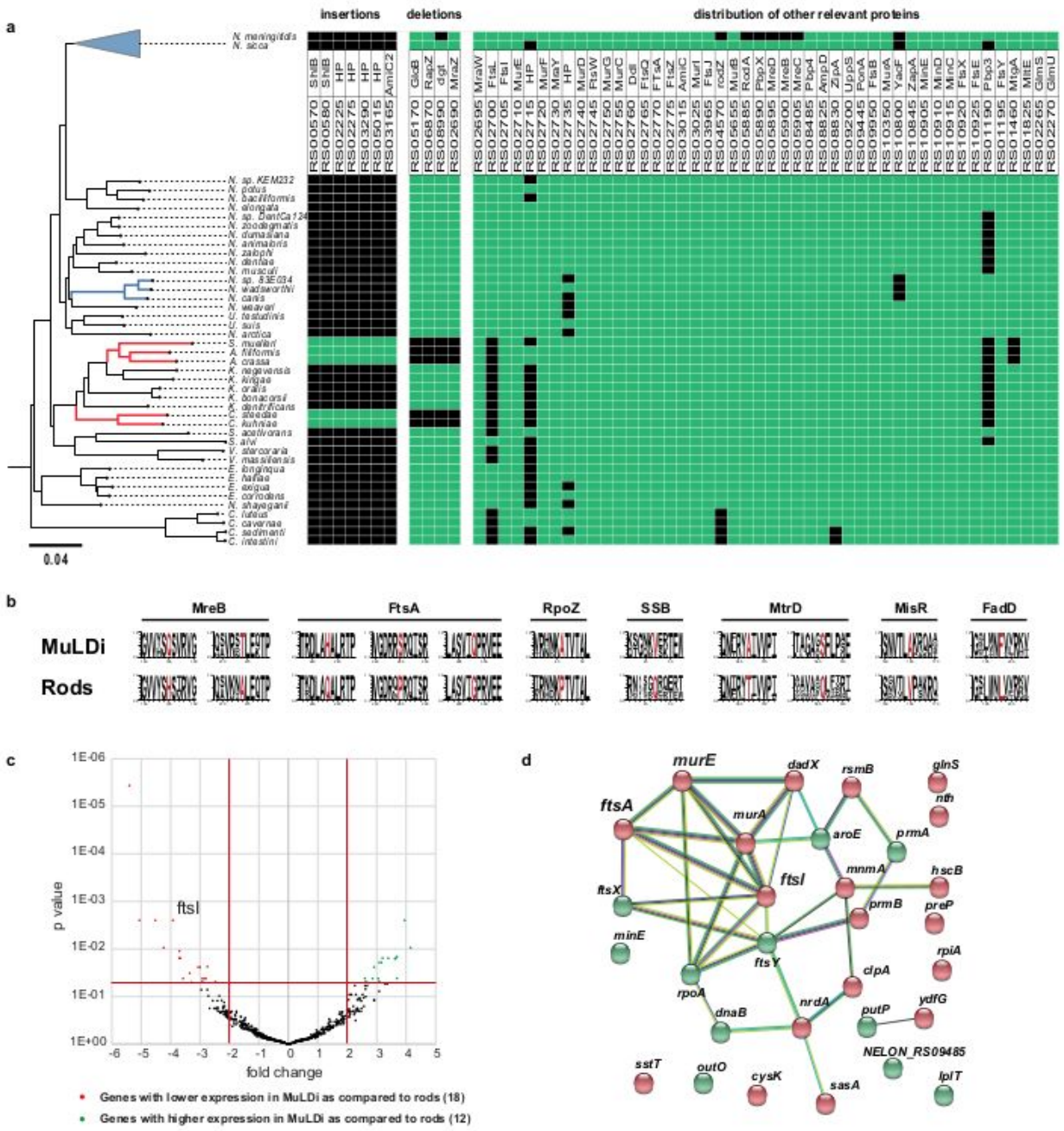

Figure 4

Comparative genomics and transcriptomic of rod-shaped and MuLDi *Neisseriaceae*.

(a) Phylogenetic tree of *Neisseriaceae* species (left) and distribution, within the family, of the genes that were inserted (left part of the table) or deleted (middle part of the table). In addition, selected proteins known to be involved in cell growth and division are also presented (right part of the table). Inserted genes are indicated with *S. muelleri* locus_tag (such as RS00570 for BWP33_RS00570). All the other genes are indicated with *N. elongata* locus_tag (such as RS02740 for NELON_RS02740). The putative encoded protein associated with each gene are also specified (HP stands for hypothetical protein). The

green and black squares of the table indicate genes that are present or absent, respectively. Individual genes were considered to be present when they had a sequence similarity ≥60% relative to *N. elongata* [an e-value cut-off of 1e-10 has also been applied in TBLASTN version 2.7.1 (Altschul et al., 1997). (b) Weblogo of the amino acid sequences, of the 7 proteins displaying amino acid permutations rod-shaped or for MuLDi, detected with amino-acids permutations between rod-shaped and MuLDi Neisseriaceae. (c) Volcano-plot: p value have been plotted with fold change. Points coloured in red are genes with lower expression in MuLDi and green correspond to genes with higher expression. (d) STRING association analysis. *ftsA*, *ftsI* and *murE* from the *dcw* cluster are highlighted. In red are genes with lower expression in MuLDi and in green are genes with higher expression.

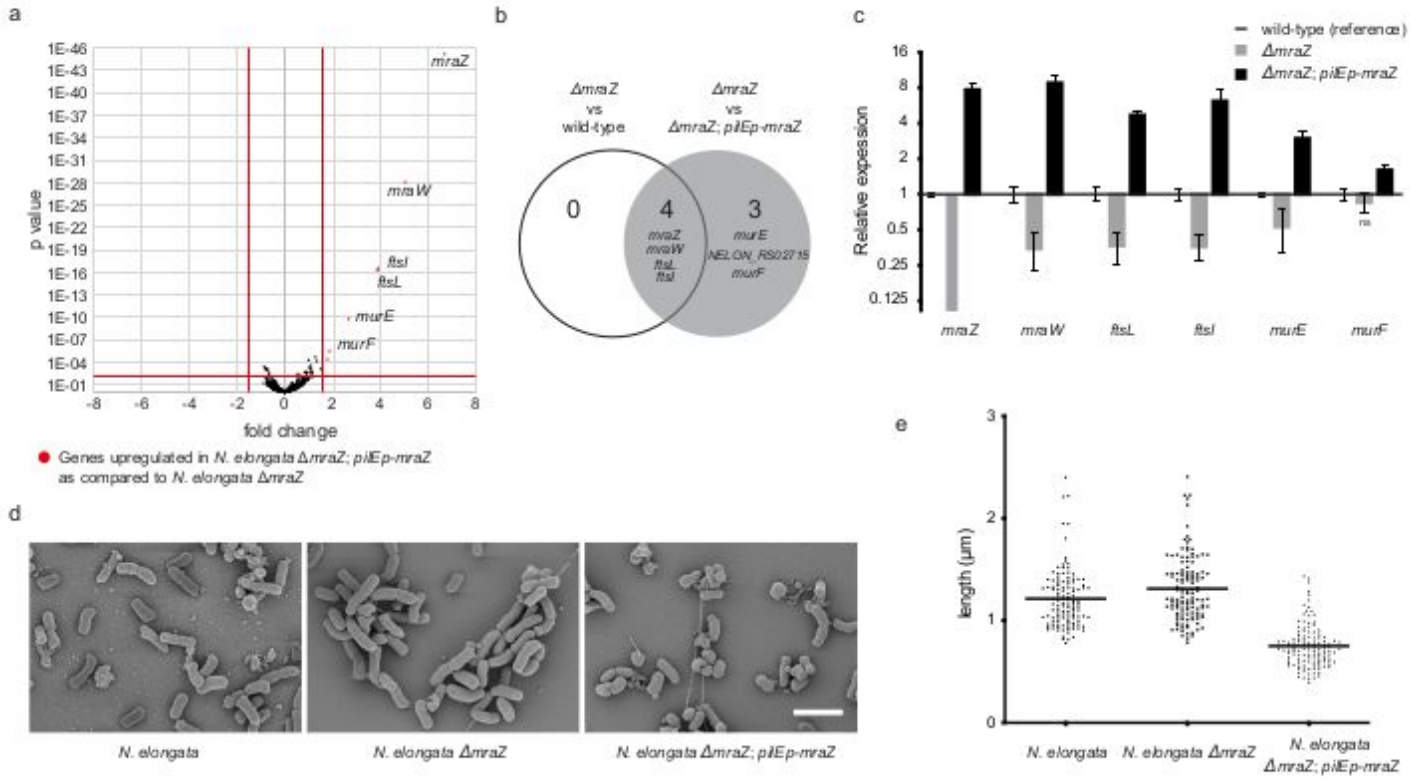

Figure 5

Downregulation of the *dcw* cluster in *N. elongata* Δ*mraZ*. (a) Volcano plot of RNAseq analysis of an *N. elongata* Δ*mraZ* and complemented. p value is plotted against fold change. Red points represent genes with higher expression in MraZ-overexpressing *N. elongata* (Δ*mraZ*; *pilEp-mraZ*), as compared to *N. elongata* Δ*mraZ*. (b) Venn diagram showing genes (*mraZ*, *mraW, ftsL and ftsI)* upregulated in *N. elongata* wild-type as compared to *N. elongata* Δ*mraZ*. (c) Transcript abundance of *dcw* cluster genes measured

by qRT-PCR in *N. elongata* expressing or not expressing MraZ. (d) Scanning electron microscopy and (e) cell length of *N. elongata* expressing or not expressing MraZ. Scale bar is 2 µm.

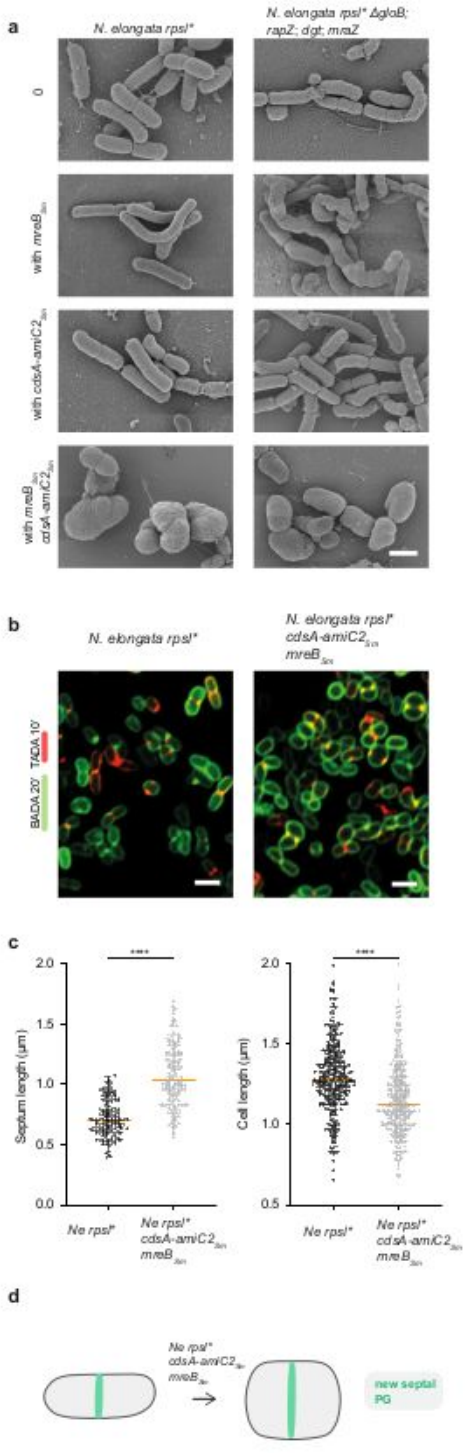

Figure 6

Recapitulation of MuLDi-specific genetic changes in the rod-shaped *Neisseriaceae N. elongata*. (a) Scanning Electron Microscopy of *N. elongata* (*rpsL**) wild-type (left panels) or harbouring multiple deletions (*ΔmraZ*, Δ*rapZ*, Δ*gloB*, Δ*dgt;* right panels), with or without the $mreB_{Ne}/merB_{Sm}$ allelic exchange, with or without the addition of *cdsA-amiC2*. (b) *N. elongata* (*rpsL**) wild-type (left) or harbouring the $mreB_{Ne}/merB_{Sm}$ allelic exchange and *cdsA-amiC2* (right) and (c) measure of the length of the septum and of the cell axis perpendicular to the septum in *N. elongata* (*rpsL**), wild-type (left) or harbouring the $mreB_{Ne}/merB_{Sm}$ allelic exchange and *cdsA-amiC2* (right). Scale bar is 1 μm. (d) Schematic representation of a septating wild-type (*rpsL**) *N. elongata* (left) and of *N. elongata* harbouring the $mreB_{Ne}/merB_{Sm}$ allelic exchange and *cdsA-amiC2* (right).

Supplementary Files

This is a list of supplementary files associated with this preprint. Click to download.

- MovieS1.avi
- MovieS3.avi
- FiguresS1S823.12.21.pdf
- NeisseriaceaeTablesS3.S6.pdf
- TablesS12221221.xlsx
- MovieS4.avi
- MovieS5.mp4
- MovieS6.mp4
- MovieS7.mp4
- MovieS2.avi